ABSTRACT

MENG, YAO. Energy Storage for Providing Regulation Service and Mitigating Power System Forced Oscillation. (Under the direction of Dr. Ning Lu).

Energy storage system (ESS) has played an important role in the operation of power grid. They ensure continuity of energy supply, improve the reliability of the system, and bring cost savings to utilities and consumers [1]. With the declination of ESS price, 1.08 Gigawatt-hours (GWh) of energy storage was deployed in the U.S. from 2013 to 2017 [2].While front-of-the-meter projects account for the majority of this capacity, behind-the-meter storage deployment is increasing. In this dissertation, two applications can potentially be provided by front-of-the-meter ESS are investigated.

Ancillary services such as frequency regulation are required for reliable operation of the electric grid. Traditionally, regulation services are provided by generators. In recent years, with the penetration level of wind and PV increases rapidly, both the ramp rate and capacity requirements of load balancing services increase significantly, causing an excess amount of large ramping actions on generator units. Instead, using high power energy storage resources to provide regulation services can reduce the wear-and-tear cost of traditional generators, as well as improve the service quality. In the first part of the dissertation, the feasibility of using ESS to provide regulation service is analyzed. A cost benefit study is conducted, in which the impact of lifetime depreciation characteristics and regulation signal design on ESS service lifetime depreciation, service quality and service costs are quantified. Then an energy storage friendly regulation signal design method based on empirical mode decomposition (EMD) is proposed. Existing designed ESS-friendly regulation signal is filter-based and does not guarantee the resultant fast changing signal is energy neutral. The advantage of using the EMD-based approach is that the regulation signal can be decomposed into a fast changing part with zero local mean and a slow-changing part

reflecting the overall trend. Regulation and price data published by New York Independent System Operator and PJM are used to conduct the study.

In the second part of the dissertation, I focused my effort on mitigating power system forced oscillation utilizing ESS. To effectively leverage the control capability offered by ESS to mitigate forced oscillations and eliminate the external disturbance ultimately, precisely locating low-frequency oscillation sources is needed. Using synchrophasor measurements, a machine learning method is proposed to locate the source of forced oscillation in power systems. Sequential feature selection is used to identify the most informative measurements of each power plant so that multivariate time series (MTS) can be constructed. We first train Mahalanobis matrix, thus the distance between the MTSs can be measured and compared. Then, we construct templates for representing each class so that the size of training datasets can be reduced and the online matching efficiency be improved. We also apply dynamic time warping (DTW) to align the MTSs that are either out of sync or with different lengths because of oscillation detection delays. The algorithm is validated on three IEEE standard system.

Energy Storage for Providing Regulation Service and Mitigating Power System Forced Oscillation

by
Yao Meng

A thesis submitted to the Graduate Faculty of
North Carolina State University
in partial fulfillment of the
requirements for the degree of
Doctor of Philosophy

Electrical Engineering

Raleigh, North Carolina

2019

APPROVED BY:

_____	_____
Dr. Ning Lu Committee Chair	Dr. David Lubkeman
_____	_____
Dr. Mesut Baran	Dr. Yunan Liu

DEDICATION

To my mother Aili Zhang, my father Qingsheng Meng

BIOGRAPHY

Yao Meng was born in Henan, China. He received his B.S. degree in Automation from Huazhong University of Science and Technology, Wuhan, China in 2012 and the M.S. degree in Electrical Engineering from Zhejiang University, Hangzhou, China in 2015. He is currently pursuing the Ph.D. degree in electrical engineering at North Carolina State University, Raleigh, NC. His current research interests include developing and applying machine learning, data analytics in power system and energy storage system application.

ACKNOWLEDGMENTS

I would like to show my sincerest gratitude to my advisor, Dr. Ning Lu. Dr. Ning Lu is an exceptional scientist and engineer with broad knowledge, strong insight, and practical skills. At the meantime, she is a great mentor with incredible patience. Without the invaluable advice she provided me on research, presentation, technical writing, and many other aspects, I wouldn't have grown and learned as much as I have.

My great appreciation and thankfulness also goes to my committee members: Dr. David Lubkeman, Dr. Mesut Barab, and Dr. Min Chi, for their time, valuable suggestions and help. I would also like to thank my mentors and colleagues in GEIRI North American Institute, ABB Corporate Research Center United States, and National Renewable Energy Laboratory during internships. It is a great pleasure to work with all of you.

I am deeply grateful to all my labmates in GridWrx for their support, encouragement, and assistance: Ming Liang, Jiyu Wang, Xiangqi Zhu, David Mulcahy, Catie McEntee, Fuhong Xie, and Mingzhi Zhang. The talks and discussions with them brought me much inspiration for my research.

Finally, I would like to thank my parents for their love and support since my birth. Thanks for standing by me all the times, joining me in a taste of all the bitters and sweets of life as a Ph.D. student. None of these would have been possible without their love and support throughout my entire life.

TABLE OF CONTENTS

LIST OF TABLES vii
LIST OF FIGURES viii
LIST OF ABBREVIATIONS xi
CHAPTER 1 INTRODUCTION 1
1.1 Overview of ESS 1
1.2 Frequency Regulation Service 6
1.3 Forced Oscillation and Its Countermeasures 8
CHAPTER 2 STUDY ON ESS PROVIDING REGULATION SERVICE 11
2.1 Background 11
2.1.1 Regulation Service 11
2.1.2 Advantages of Using ESS to Provide Regulation Service 14
2.1.3 Pay-for-Performance Market Mechanism 16
2.2 Modeling of ESS 20
2.2.1 ESS Operation Model 20
2.2.2 ESS Lifetime Estimation 21
2.3 Cost-Benefit Study for ESS Providing Regulation Service 22
2.3.1 Modeling Methods 22
2.3.2 Simulation Results 24
2.3.3 Conclusions 30
2.4 Regulation Signal Design Using Empirical Mode Decomposition 32
2.4.1 Modeling Methods 33
2.4.2 EMD-Based Regulation Signal Design 36
2.4.3 Case Study 40
2.4.4 Conclusions 47
CHAPTER 3 MITIGATION OF POWER SYSTEM FORCED OSCILLATION 48
3.1 Introduction 48
3.1.1 Low Frequency Oscillation 48
3.1.2 Mechanism of Forced Oscillation 49
3.2 Damp Forced Oscillation with ESS 51
3.3 Forced Oscillation Source Location 56
3.3.1 Data Preparation 59
3.3.2 Modeling Methods 60

3.3.3 Numerical Experiments 69
3.4 High-Efficiency Forced Oscillation Source Location..... 74
3.4.1 Template Classification 75
3.4.2 Numerical Experiments 78
3.4.3 Conclusions..... 86
CHAPTER 4 SUMMARY..... 88
REFERENCES 91

LIST OF TABLES

Table 2. 1 Regulation reserve requirement. 14

Table 2. 2 Storage characteristics. 23

Table 2. 3 Storage cost parameters. 28

Table 2. 4 Performance comparison when using different types of regulation signals and charging methods. 29

Table 2. 5 EMD based regulation signal design. 40

Table 2. 6 HRR parameters. 41

Table 2. 7 Performance comparison of battery. 43

Table 2. 8 Performance comparison. 46

Table 3. 1 Mahalanobis matrix training algorithm 66

Table 3. 2 Performance test of oscillation source identification for four-machine two-area model. 72

Table 3. 3 Performance test of oscillation source identification for IEEE 39-bus system. 73

Table 3. 4 Template generation. 76

Table 3. 5 The performance of different number of templates. 83

LIST OF FIGURES

Figure 1. 1 Energy storage deployment across the United States in 2017 [8]. 3

Figure 1. 2 Dissertation framework. 6

Figure 1. 3 Illustrative data related to frequency regulation. (a) The NY-ISO ACE signal (June, 2017); (b) corresponding PDF of NY-ISO ACE over one week; (c) one hour NY-ISO regulation signal; and (d) one hour PJM RegD signal [10], [11]. 8

Figure 2. 1 Control continuum [20]. 12

Figure 2. 2 Illustration of the real-time control process [21]. 13

Figure 2. 3 Duration curves of estimated hourly regulation requirements for load and selected wind scenarios. 15

Figure 2. 4 (a) Regulation service provided by a conventional generator, and (b) regulation service provided by energy storage [24]. 16

Figure 2. 5 Design of fast regulation signal [28]. 17

Figure 2. 6 PDF of PJM RegA hourly energy bias during June–August 2017; (b) PDF of PJM RegD hourly energy bias during June–August 2017. 18

Figure 2. 7 An example of regulation capacity and mileage. 20

Figure 2. 8 Storage cycles over its life versus depth of discharge (DOD). 22

Figure 2. 9 Daily revenues for providing 2017 NYISO regulation signals. 25

Figure 2. 10 Comparison of daily revenue across the year, associated with following different signals. 26

Figure 2. 11 Comparison of daily response rate. 27

Figure 2. 12 Comparison of lifetime depreciation. Note that aging cost is the percentage of life reduction after one day of service. 27

Figure 2. 13 Comparison of Lithium-ion and flywheel net benefit for 1-directional and 2-directional services. 28

Figure 2. 14 Comparison of net annual benefits for different battery sizes. 30

Figure 2. 15 High-level conditional neutrality controller [40]. 35

Figure 2. 16 Block diagram of the generator model. 36

Figure 2. 17 One day regulation signal and its IMF components. 42

Figure 2. 18 Simulation results of hydro response: (a) Hydro generator responds to RegA signal, (b) Hydro generator responds to EMD_slow signal. 44

Figure 2. 19 Regulation signal required and the regulation service provided. 45

Figure 3. 1 SMIB system with E-STATCOM. 52

Figure 3. 2 Equivalent circuit of SMIB system with E-STATCOM [19]. 52

Figure 3. 3 Block diagram of SMIB system with E-STACOM. 53

Figure 3. 4 Block diagram of suppression method [19]. 54

Figure 3. 5 Simulation results, where the subscripts Y and N denote the ones with and without the proposed method, respectively [19]. 56

Figure 3. 6 Dataset Generation. 59

Figure 3. 7 Training and testing data set illustration. 67

Figure 3. 8 An optimal warping path. 69

Figure 3. 9 Excitation system of source generator. 70

Figure 3. 10 IEEE 39-bus system. 72

Figure 3. 11 The relationship between location accuracy and the time delay. 74

Figure 3. 12 Template generation process. 76

Figure 3. 13 Flowchart of forced oscillation source identification based on multivariate time series classification. 78

Figure 3. 14 WECC-179 bus system. 79

Figure 3. 15 Simulated PMU measurements. (a) Absolute angle of G1 with disturbance injected at different generators; (b) Absolute angle of G1 with disturbance injected at G1 for different load fluctuations. 80

Figure 3. 16 Precision of classification for ideal case. 82

Figure 3. 17 Precision and execution time for different number of templates. 84

Figure 3. 18 Precision of classification over different *d*. 85

Figure 3. 19 Process to add harmonic oscillation source. 86

LIST OF ABBREVIATIONS

ESS	Energy Storage System
PSH	Pumped Storage Hydro
TOU	Time-of-Use
ACE	Area Control Error
PDF	Probability Density Function
CPS	Control Performance Standard
NERC	North American Electric Reliability Council
EMD	Empirical Mode Decomposition
PSS	Power System Stabilizer
STATCOM	Static synchronous compensator
MTS	Multivariate Time Series
DOD	Depths of Discharge
SOC	State of Charge
NPV	Net Present Value
EAA	Equivalent Annual Annuity
IMF	Intrinsic Mode Functions
HRR	Hybrid Regulation Resource
MAE	Mean Absolute Error
SMIB	Single-Machine Infinite-Bus
PMU	Phasor Measurement Unit
DTW	Dynamic Time Warping
PSD	Positive Semi-Definite

LMIs	Linear Matrix Inequalities
KNN	K-Nearest Neighbors
BESS	Battery Energy Storage System
DBSS	Distributed Battery Storage System
HIL	Hardware-in-the-loop
PDNO	Poorly Damped Natural Oscillation
FO	Forced Oscillation

CHAPTER 1 INTRODUCTION

1.1 Overview of ESS

There are multiple forms of energy, certain forms of energy can be transferred conveniently but hard to store, such as electricity. While some forms are the other way around, like chemical, kinetic, etc., difficult to be transmitted but easily to be stored. ESS converts energy from forms that are difficult to store to more conveniently or economically storable forms. In power system, ESS is a system used to store electrical, mechanical, chemical, or thermal energy that was once electrical energy, for use in a process that contributes to end-user demand management or grid operation and reliability [2]. Ideally, power supply and demand should be equal at any given moment in electricity grid. However, there would be unexpected changes on both supply and demand side, like generators trip/natural disaster, it's impossible to maintain the balance between electricity generation and consumption constantly only by advance arrangement. ESS can be a viable and ideal approach to deal with this balancing problem, which is essential to the operation of power systems. For example, when there is more electricity generated than needed, such as during the mid-night when low-cost power plant continues to operate while the demand is extremely small, ESS can absorb excess electricity generation. On the contrary, when demand is greater than supply, ESS can discharge the stored energy to support the grid.

Renewable energy, like wind and solar, can certainly provide us a sustainable energy future while reducing greenhouse gas emissions. However, the intermittency and uncertainty in its power output pose the barrier to its further implementation. ESS can smooth out the power generation by renewable energy resources, which enables their large-scale applications. What's more, ESS controlled by power electronic devices, like battery and flywheel, can have a very high ramping rate. Typically, the output of ESS can vary from zero to its rated power in less than one second,

while conventional generators need to take much longer to ramp up. This fast response helps the grid become more flexible and reliable by dealing with unexpected changes in time. With the increase in renewable penetration [4] and the rapid decrease in ESS manufacturing cost [5], the installation of ESS in power system is increasing rapidly [6]. The research on how to utilize ESS effectively and efficiently is in great need.

During 2013 to 2017, 1.08 Gigawatt-hours of ESS has been deployed in the U.S. [7]. Most of the capacity is installed as grid-connected device, while behind-the-meter storage installation is increasing. For example, in quarter 1, 2018, behind-the-meter ESS installations accounted for 63% of the MW and 49% of the MWh deployed. ESS deployment tends to be concentrated in several states, mainly due to ESS friendly market mechanism and high demand. As shown in figure 1.1, PJM market and California ISO are two main areas with ESS deployment, installed capacity as 278 MW and 130 MW, respectively.

As mentioned before, there are multiple forms of energy, accordingly there are bunch of energy storage technologies available today. Considering the form of stored energy, we have divided energy storage technologies into five main categories: electromechanical, electrochemical, chemical, thermal, and electrical [2]:

Electromechanical： Convert electricity into mechanical form, such as kinetic energy, for example flywheel and compressed air energy storage; or gravity potential, like pumped storage hydro (PSH). PSH is a mature technology and the largest installed storage system in U.S. However, its deployment is restricted by the geographical condition.

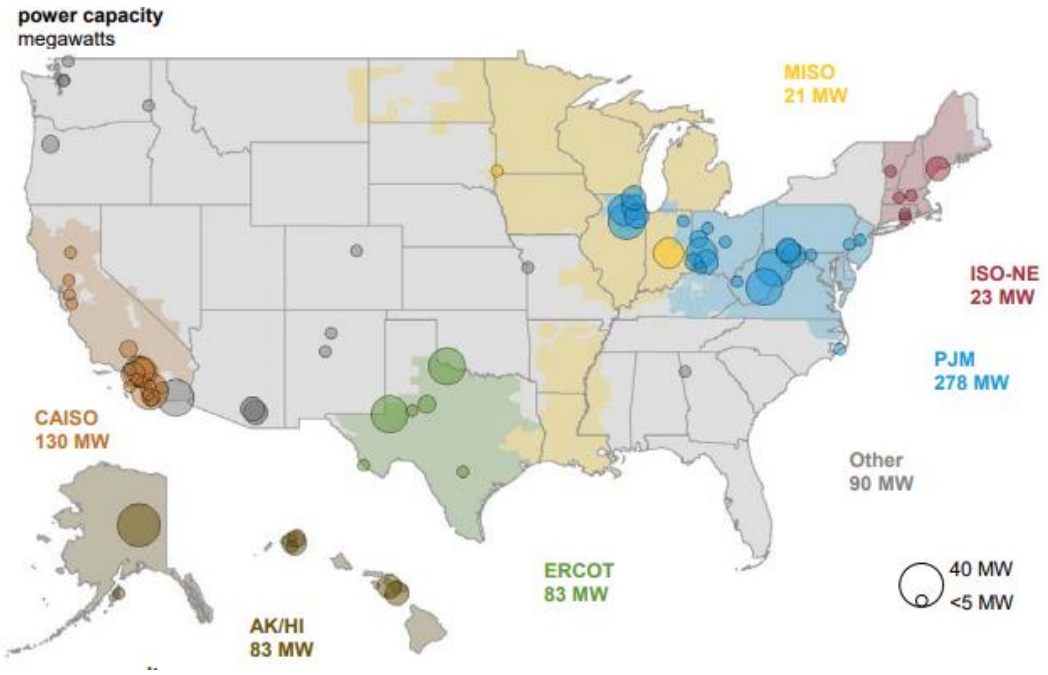

Figure 1. 1 Energy storage deployment across the United States in 2017 [8].

Electrochemical： This technology stores electricity under a chemical form, which mainly refers to rechargeable battery, such as lead acid battery, lithium-ion battery. Its realization is based on the fact that both electrical and chemical energy share the same carrier-electron.

Chemical： This technique stores energy in chemical fuels, the main process is transforming electrical power into gaseous fuel, such as hydrogen and synthetic methane. Later the gas can be used to power gas turbines.

Thermal： This technology captures heat and cold to create energy on demand. It is the temporary storage or removal of heat. Existing methods include water heaters, ice storage and chilled water storage.

Electrical： This technique stores energy in electricity form directly, such as super capacitors and superconducting magnetic energy storage. Typically, these methods can't store the energy for a long time, but they can provide a short burst of energy in milliseconds.

In this dissertation, we conduct study on utilizing ESS to provide regulation service and mitigate forced oscillation in power grid, which requires a fast ramping rate of ESS. Thus the storage technologies we consider are lithium-ion battery and flywheel.

Typically, grid-connected and behind-the-meter ESS can provide different services. Behind-the-meter services are also called end-user services:

Time-of-Use/Energy Management： ESS can store electricity from power grid for a later use. This enables customers to take advantage of time-of-use (TOU) rate.

Demand Charge Management： By shifting electricity consumption to reduce the use during grid peak period, ESS can reduce demand charge.

Backup Power： When power outage occurs, ESS can provide power to the end-users who disconnected from the power grid.

Power Quality Management： For the users who require highly conditioned power, ESS controller can monitor the operation condition of power grid and improve the power quality, like reducing voltage fluctuation, counteracting voltage drop.

Typically, there are three main categories of services that grid-connected ESS can provide, include distribution services, transmission services, generation and resource adequacy services [3]:

Distribution Services： 1.Voltage support and control, ESS can be used to improve voltage quality by smoothing voltage flicker, maintaining voltage within industry limits across distribution circuits; 2. Reliability enhancement, ESS can be utilized to support microgrid during islanding or distributed energy resources to enhance the reliability of distribution circuit; 3. Capacity deferral and peak shaving, ESS can be utilized to defer expensive substation and distribution feeder upgrades, reduce peak demand, and help to support operation of the sub-transmission and transmission systems.

Transmission Services： 1. Transmission investment deferral, ESS can provide power capacity in locations where need additional transmission capacity to serve peak load for a certain period of time; 2. Transmission congestion relief, ESS can relieve transmission congestion and allow less expensive generators or renewable generators to produce more energy.

Generation and Resource Adequacy Services： 1. Peak capacity deferral, electricity generated at non-peak demand periods can be stored in ESS and then injected at peak demand periods to decrease peak generation capacity requirements; 2. Bulk energy time shifting, the electricity production time can be shifted with ESS; 3. Frequency regulation, ESS with fast response can provide primary and secondary frequency regulation by following a fast-changing instructional signal; 4. Reserves, serve as spinning and non-spinning reserves to support contingency events and large imbalances between supply and demand; 5. Black start capacity, the energy stored can be used to restart the grid in the event of bulk system blackouts; 6. Flexible ramping, ESS reduces the need for conventional generators to ramp quickly in response to diurnal demand profiles and variable generation from renewable resources; 7. Synthetic inertia, control systems with ESS can provide fast response that mimic inertia responses of generators.

Since ESS has fast ramp rate, it is suitable to provide support to maintain the balancing and stability of power system. In this dissertation, two applications potentially can be provided by ESS are investigated. An outline of the research works is shown in figure 1.2. Frequency regulation maintains the minute-to-minute balance and is used to maintain the balance between load and generation and restore frequency to its scheduled value, *i.e.* 60 Hz in U.S.. This service requests provider change its power output in a high time resolution, typically in seconds. However, traditional generator with relatively low ramp rate can hardly satisfy this requirement. Thus the feasibility, economic and possible problems of utilizing ESS to provide regulation service are

analyzed in the first part of this dissertation. Forced oscillations (FO) caused by resonance have been discovered recently, which have different mechanism from poorly damped natural oscillation (PDNO). Thus, the countermeasure for PDNO-typically increasing the system damping, doesn't work for FO. With the high ramp rate, ESS provides a viable way to reduce the damage from FO by absorbing the oscillation energy, thus buy time to locate and remove the oscillation source ultimately. In the second part of the dissertation, the possibility of using ESS to mitigate FO is investigated. Then a machine learning based FO source location approach is proposed to completely solve the FO problem. Detailed description and the state of art for each work will be introduced in the following part respectively.

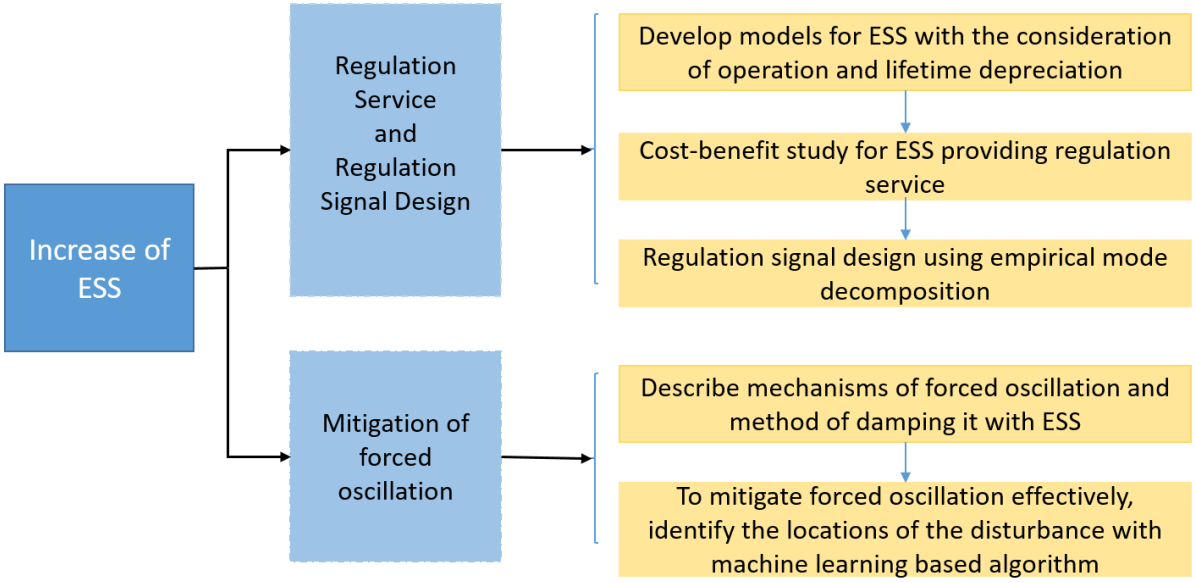

Figure 1. 2 Dissertation framework.

1.2 Frequency Regulation Service

The operation of the electric power system needs to maintain a continuous balance between generation and load. Frequency regulation is an important component of operating reserves used to maintain this balance. When load increases or decreases suddenly, system frequency will decrease or increase. The rate of frequency change depends on system inertia. During such a

change, generator governors respond and adjust the generation to match the load changes in order to bring the system frequency to a new equilibrium point.

To restore the system frequency to its nominal value (i.e., 60 Hz in the U.S.) and to maintain tie-line power flows between different control areas at scheduled values, frequency regulation is performed, consisting of small increases (i.e., regulation up) and decreases (i.e., regulation down) in power output by participating resources [9]. In general, the frequency regulation signal is generated from a designed controller with the Area Control Error (ACE) as the controller input and usually updated every 2-10 seconds. Figure 1.3 provides an example of ACE signals in NY-ISO, its corresponding probability density function (PDF) over one week, the NY-ISO regulation signal, and PJM RegD signal.

Derived from ACE signals, regulation signals usually bear the same characteristics as the ACE signals. As shown in figure 1.3(b), although the mean value of the ACE signal is very close to zero in a window of 24-hour, it can have a large bias over a given period of time (e.g., between hour 25 and 30 in figure 1.3(a)). The regulation signals are always proportionally scaled with respect to the capacity of participating units, which are in the range of $[-1,1]$, as shown in figure 1.3 (c)-(d).

The main reasons for performing regulation are to maintain the grid frequency and to comply with the North American Electric Reliability Council (NERC) Control Performance Standards 1 and 2 (CPS1 and CPS2) [12]. These two standards require the minimum control level for ACE in each control area so that areas manage their own load changes. CPS1 requires that the ACE for a control area be in the direction to bring the frequency back towards its scheduled value, at least a certain fraction of the time. CPS2 limits the average value of ACE over each 10-minute period for each area, to ensure that the total load-generation imbalance for the area does not tend

to be too large in magnitude. In this dissertation, a cost benefit study of using ESS to provide regulation services is presented. The impact of lifetime depreciation characteristics and regulation signal design on ESS service lifetime depreciation, service quality and service costs are quantified. Then a regulation signal design algorithm based on empirical mode decomposition (EMD), for dispatching regulation services between slow and fast responding resources is proposed.

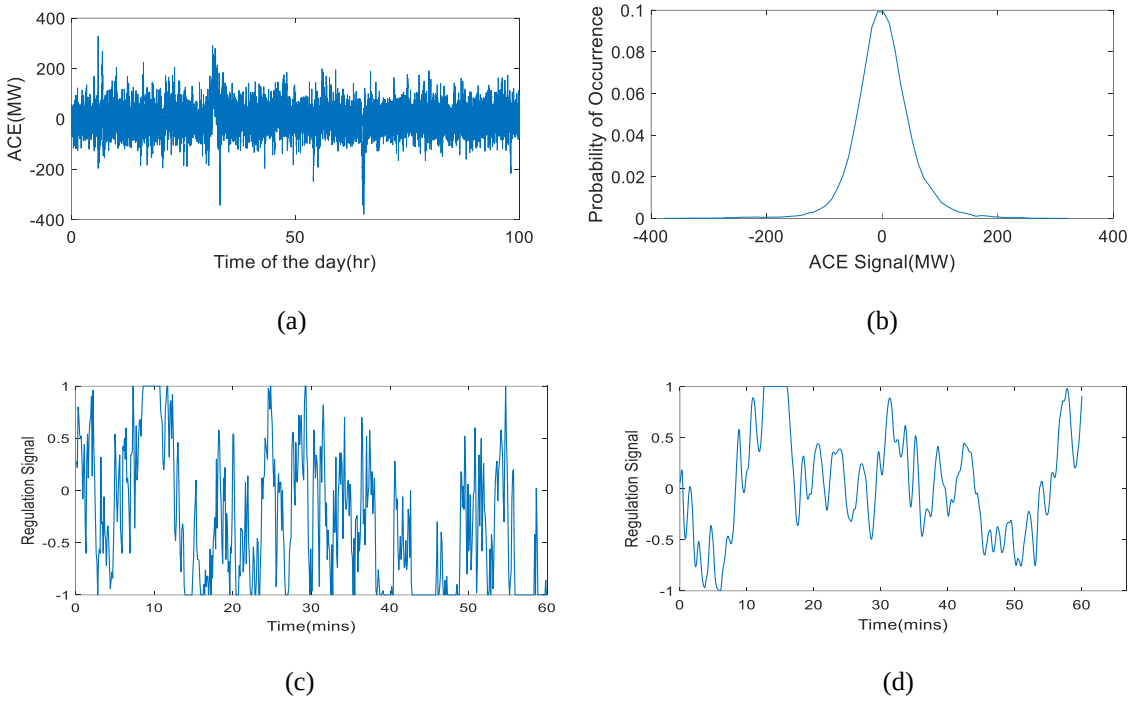

Figure 1. 3 Illustrative data related to frequency regulation. (a) The NY-ISO ACE signal (June, 2017); (b) corresponding PDF of NY-ISO ACE over one week; (c) one hour NY-ISO regulation signal; and (d) one hour PJM RegD signal [10], [11].

1.3 Forced Oscillation and Its Countermeasures

As a complex and nonlinear system, power grid suffers a number of instability problems. If one looked back the history of power system since its evolution, operation engineers faced with transient instability problem and researchers struggled to find counter measures to overcome it [12]. Transient stability is defined as the ability of power system to maintain synchronism when subjected to large disturbances, for example loss of tie lines, loss of main generators. After large

disturbances occurred, well-designed system would approach back to equilibrium, which is a normal phenomenon called damped oscillation. However, improper operating conditions, external fluctuation forces may lead to sustained oscillations, which will reduce power transmission limit and may lead to damage of system equipment. It severely threatens the security and stability of large-scale interconnected power systems in real-time operations.

In the current literature, two types of mechanisms for sustained oscillations, i.e. PDNO and FO, have been extensively investigated and explained for observed oscillation events [14]. Insufficient damping of a system results in a majority of low-frequency oscillation, which is called PDNO. This kind of oscillation can be suppressed by tuning parameters of power system stabilizer or intertie line controls. FO caused by resonance have been discovered recently [15] in power grids. The posterior analysis shows the system was well damped when the oscillation occurred. Moreover, disturbance with a frequency approximating the intrinsic system frequency was injected into the power system somewhere. The resonance excited and even the small disturbance could amplify and spread rapidly in the whole power system. The traditional remediation actions, for example putting power system stabilizers into operation, etc., are not applicable for suppressing such oscillations. The most effective way to quench FO is to remove the disturbance rapidly and accurately.

Unlike PDNO, which will attenuate quickly by improving the damping with power system stabilizers (PSS) or FACTS-based stabilizers, FO still happen and sustain with the appearance of external fluctuation forces even the system is with good damping characteristics [16]. The only way to completely solve FO is to remove the external disturbance. However, the prerequisite to eliminating the disturbance is accurate oscillation source localization, which needs exectution time. Static synchronous compensator (STATCOM) has been applied to suppress low-frequency

oscillations, however its mitigation ability is limited by the restriction of voltage amplitude [17], which makes it less effective for FO driven by persistent disturbance. By incorporating energy storage unit with STATCOM, E-STATCOM is obtained, which is more powerful for dealing with FO [18]. With the help of E-STATCOM, FO propagating from the disturbed generator/area to the rest of power grid can be eliminated timely [19], ensure no detrimental consequences occur during the time period needed for locating the external disturbance. To use energy storage unit effectively and efficiently, a machine learning method is proposed to locate the source of forced oscillation in power systems using synchrophasor measurements. Selected PMU measurments of each power plant are utilized to construct multivariate time series (MTS). Applying Mahalanobis distance metric and dynamic time warping, the distance between MTS with different phases or lengths can be appropriately measured. The obtained distance metric, representing characteristics during the transient phase of FO under different disturbance sources, is used for offline classifier training and online matching to locate the disturbance source.

CHAPTER 2 STUDY ON ESS PROVIDING REGULATION SERVICE

This chapter introduces the study on utilizing ESS to provide regulation service. To guide the deployment of ESSs, the ESS performance and cost-of-service when providing different types of regulation signals are quantified. Then a regulation signal design algorithm considering the characteristics of regulation market participating resources will be demonstrated correspondingly.

2.1 Background

This section is organized as follows. Sub-section 2.1.1 introduces the regulation service. Sub-section 2.1.2 illustrates characteristics of ESS and its advantages for providing regulation service. Sub-section 2.1.3 presents the pay-for-performance market mechanism of regulation service.

2.1.1 Regulation Service

Each balancing authority maintains the frequency by monitoring ACE and keeping the value within limits. In reality, the frequency control is realized through utilizing different resources or market products, as shown in figure 2.1.

Primary control is also called frequency response, which occurs within the first few seconds when there is a change in system frequency, *i.e.* disturbance, to stabilize the interconnection. Frequency response is usually provided by the action of generator governor and the shedding of system load. Primary control is maintained until it is replaced by AGC action;

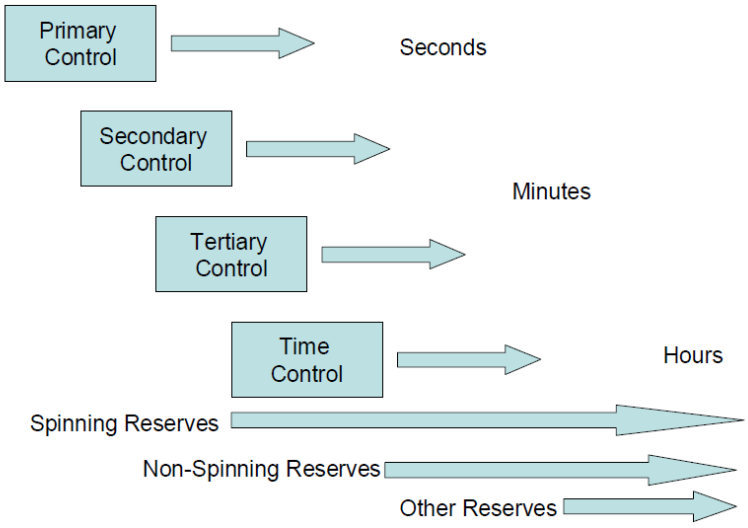

Figure 2. 1 Control continuum [20].

Secondary control includes the balancing services deployed in minute time frame, where regulation service falls in this category. The most common means of exercising secondary control is through automatic generation control (AGC).

Tertiary control is used to handle current and future contingencies by getting resources in place. Common types of tertiary control include reserve deployment and reserve restoration.

Time control is used to maintain the long-term average frequency at 60 Hz. Since frequency and balancing control are not perfect, there will always be occasional error, which means that frequency cannot always be maintained at exactly 60 Hz.

All ISO/RTOs acquire regulation capacity in their day-ahead (DA) and real-time (RT) markets. The purpose of regulation is to maintain power balances within the final real-time interval (e.g., 5 minutes in CAISO and MISO) based on four-second signals from the system operator. Meanwhile, the CAISO and MISO have both implemented flexible ramping products (FRP) in their respective operational frameworks to better utilize the ramping capability from existing generators and respond to variable renewable ramping events. Once the generators are scheduled to meet forecast ramping needs, any finer fluctuations within a dispatch interval are left to be

picked up by the regulating units. Renewable generation, such as wind and photovoltaic (PV) solar power, increases the amount of variability and uncertainty on power systems. Define net load as the total electric demand in the system minus wind and solar generation. As shown in figure 2.2, the solid line is the actual net load, the dashed line is 5-min schedule, the difference between the actual net load curve and the 5-minute net load forecast is net load deviation, which is covered by the procured regulation reserve within 5-minute interval. Thus, regulation service is utilized to cover: 5-minute net load forecast error and second-to-second load variation. Since these two factors occur in a fine time frame (second), traditional generators can't follow them perfectly.

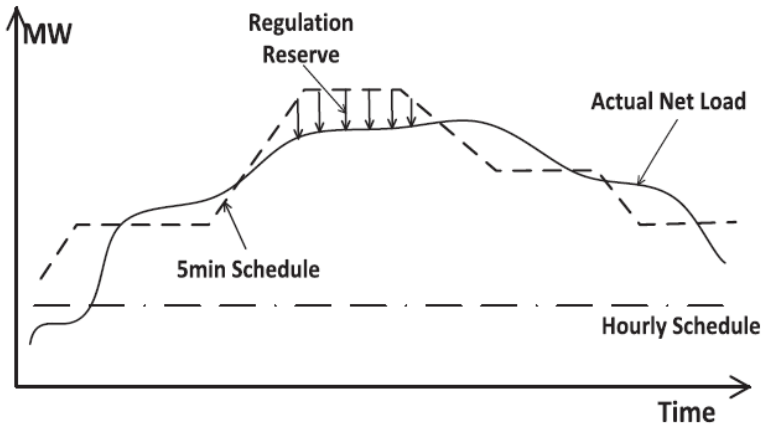

Figure 2. 2 Illustration of the real-time control process [21].

On the other hand, the regulation requirement is hard to be estimated. As listed in table 2.1, the balancing authorities decide the regulation requirement with rough estimation. Moat of these methods are based on rules of thumb. For example, in PJM regulation capacity for each hour are selected from two quantities, i.e. 525 MW and 800 MW. While, Many properties of a power system—including its generation levels, load levels, and transmission equipment availability—are both variable and uncertain. Thus, the estimation can hardly meet the real regulation requirement. To improve the quality of regulation service and compensate the regulation requirement estimation error, the devices with supreme ramp rate are highly desired.

Table 2. 1 Regulation reserve requirement.

Region	Regulation Requirement
PJM	1% of peak load during peak hour and 1% of valley load during off-peak hour
NYISO	Based on hour of day, weekday/weekend and season
ERCOT	Based on 98.8th percentile of regulation reserve utilized in previous 30 days and same month of previous year and adjusted by installed wind penetration
CAISO	A percentage of CAISO forecast of CAISO demand for the hour
ISO-NE	Based on hour of day, weekday/weekend and month
MISO	MISO requirement is a bidirectional value varying between 300 MW to 500 MW depending on load level and time of the day

2.1.2 Advantages of Using ESS to Provide Regulation Service

When the amount of renewable generation increases, the need for regulation and load following services will increase. In December 2010, ISO-NE released the final report of its New England Wind Integration Study [22]. The study assessed a number of growth scenarios for wind in New England up to year 2020, and the potential impacts on the ISO-NE power grid. As shown in figure 2.3, the study identified a need for an increase in the regulation requirement even in the lowest wind penetration scenario (2.5% wind energy), and the requirement would have noticeable increases for higher penetration levels. For example, the regulation requirement increases to 161 MW in the 9% wind energy scenario (about 4000 MW of wind), and to as high as 313 MW in the 20% scenario (8000-10000 MW).

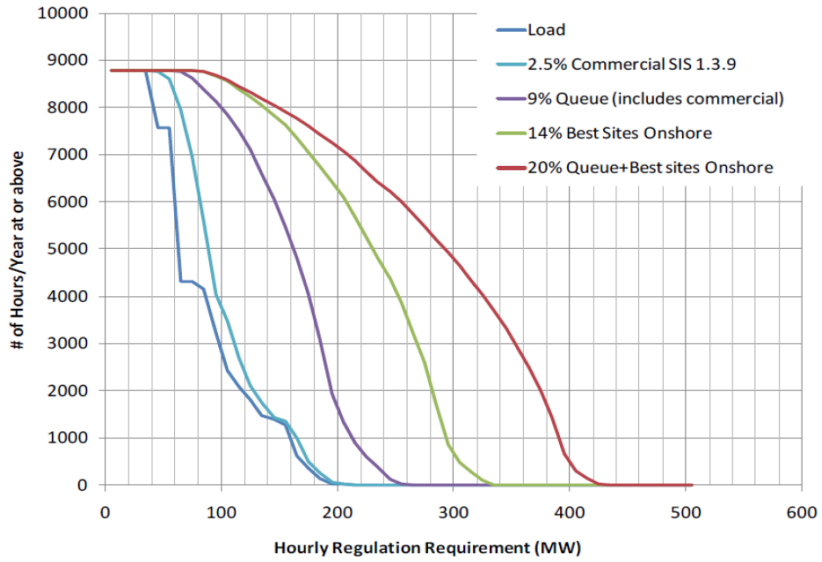

Figure 2. 3 Duration curves of estimated hourly regulation requirements for load and selected wind scenarios.

Traditionally, regulation services are provided by generators. Providing regulation services reduces generator lifetime because of the significant wear-and-tear caused by fast ramping up and down. In power grids with high penetrations of intermittent renewable generation, both the magnitude and speed of the variations in the regulation signal are high, producing even higher wear-and-tear on the regulation units. In addition, because of the limited ramping capabilities, the response rates of conventional regulation generators are slow, as shown in figure 2.4(a). Thus, to meet regulation requirements, more regulation capacity is required to compensate the control errors.

To create incentives for fast responding resources to participate in regulation services, the Federal Energy Regulatory Commission enacted FERC Order 755 [23], which requires system operators to add a performance payment with an accuracy adjustment to the capacity payment typically used in markets for ancillary services. All ISO/RTOs have implemented this pay-for-performance regulation market. Under this new market rule, the participating resource will be rewarded by what it declares (i.e., regulation capacity) and what it supplies (i.e., regulation

mileage).

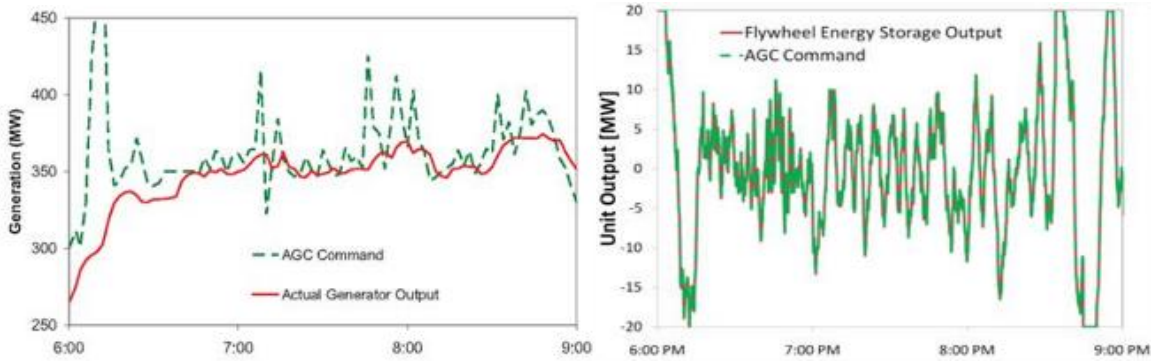

(a) (b)

Figure 2. 4 (a) Regulation service provided by a conventional generator, and (b) regulation service provided by energy storage [23].

Those regulatory advancements make providing fast regulation service a high-value ancillary service, and also make energy storage a suitable candidate for providing it. Compared with generator units, an energy storage controlled by power electronics has a fast response rate that can follow the regulation signals closely, as shown in figure 2.4(b), where the AGC command is similar with the regulation signal, derived from ACE. There are three main advantages of using energy storage for regulation services: it reduces the wear-and-tear on conventional generators, reduces the amount of required regulation capacity, and improves the quality of regulation services [25].

In the past few years, the share of energy storage in regulation markets has increased rapidly. For example, in the PJM market, the storage capacity has increased from zero in 2005 to over 280 MW in 2017, making up 41% of its regulation procurement capacity [23]. Since enabling the use of storage in its market, PJM has been able to reduce the size of its regulation market by 30%, resulting in significant savings for ratepayers.

2.1.3 Pay-for-Performance Market Mechanism

In this section, we briefly describe the regulation signals and service payment mechanism.

A.Regulation signals

ACE signals often have some DC component, so they are not energy-neutral. This can cause an energy storage system with limited energy storage capabilities to be fully charged or discharged after providing regulation services over a period of time. Thus, ISOs such as PJM and ISO-NE have designed an energy-neutral regulation signal to facilitate the provision of regulation services by storage [25]. For example, in PJM, regulation signals have been split into two signals: slow-responding Regulation A (RegA) and fast-responding Regulation D (RegD, where the D stands for "dynamic") [26]. The RegD signal is generated by applying the original PJM ACE signal to a high pass filter, as shown in figure 2.5. In this configuration of the split-signal system, RegA was designed for resources "with the ability to sustain energy output for long periods of time, but with limited ramp rates", while RegD was designed for resources "with the ability to quickly adjust energy output, but with limited ability to sustain energy output for long periods of time" [27].

Figure 2. 5 Design of fast regulation signal [28].

As shown in figure 2.6, the hourly energy bias of 1MW units responding to PJM-RegD is very close to zero while PJM-RegA has a DC bias. The PJM example demonstrates that if regulation signals are carefully designed, the disadvantage of using energy storage can be avoided. By letting energy storage devices supply the fast changing component of the regulation signal, the generator units are allowed to move slower and less, reducing their wear-and-tear while improving the regulation service quality.

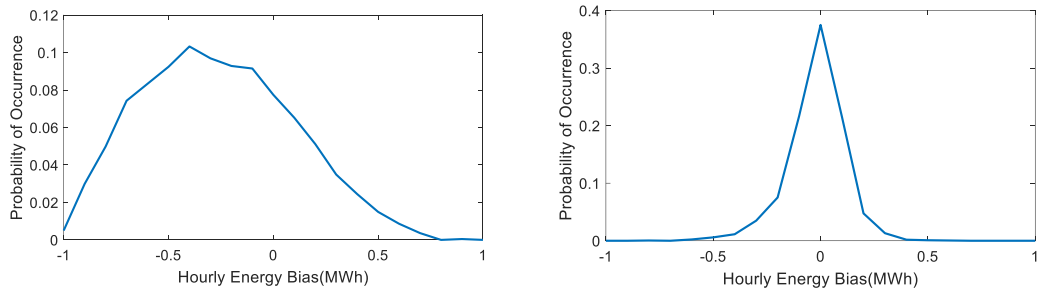

(a) (b)

Figure 2. 6 PDF of PJM RegA hourly energy bias during June–August 2017; (b) PDF of PJM RegD hourly energy bias during June–August 2017.

Thus in this chapter, we compare the use of flywheels and lithium-ion batteries in four different cases: (1) the PJM-RegD, representing ESS-friendly fast regulation signals, (2) PJM-RegA, representing a slow regulation signal, (3) PJM-RegA plus PJM-RegD, representing the original PJM regulation signals, and (4) the NYISO regulation signal. All signals are actual regulation signals downloaded from the PJM and NYISO websites.

B.Payments for providing regulation services

Following FERC Order 755, all ISO/RTOs have implemented a pay-for-performance regulation market. Under this market mechanism, participating resources are rewarded by regulation power capacity, P_{bid}^{reg} and regulation mileage, M. The capacity offering price is in \$/MWh. The unit for mileage price is \$/ΔMW. In most regulation markets, a participating unit commits a P_{bid}^{reg}, for a bidding interval with a length T. P_{bid}^{reg} is symmetrical in most ISO control areas, except in CAISO. "Symmetrical" means that the regulation-up and regulation-down signals have the same power limit of P_{bid}^{reg}. The regulation instructional signal at time t, P_t^{reg}, is a normalized percentage of P_{bid}^{reg}. To guarantee that regulation signals are within the committed regulation capacity limit of the unit, we always have:

$$\left|P_t^{Reg}\right| \leq 1 \tag{2.1}$$

Regulation mileage is the sum of absolute values of the regulation control signal movements. If the output of a regulation unit is P_t^{Reg} and the declaring regulation capacity is P_{bid}^{reg}, the regulation mileage is calculated:

$$M = \sum_0^T \frac{|P_t^{reg} - P_{t-1}^{reg}|}{P_{bid}^{reg}} \tag{2.2}$$

Usually, system operators will calculate a performance factor (λ) with a value between 0 and 1, to represent the response accuracy with respect to the regulation instructions. Depending on the market design, the performance factor is calculated and applied differently. Its purpose is to decrease the regulation payment to account for inaccuracy in response. A general penalization format is as follows:

$$\text{Payment} = P_{bid}^{reg}(\rho_c + \lambda \text{M} \rho_M) \tag{2.3}$$

where ρ_c and ρ_M represent the capacity clearing price and mileage clearing price, respectively. Since lithium-ion batteries and flywheels can have high response accuracy when providing the regulation service, we assume $\lambda = 1$, i.e., there is no payment penalization.

Figure 2.7 shows an example of the energy storage power outputs when responding to regulation signals. The regulation-up capacity is equal to the regulation-down capacity (i.e. ±1MW), as shown by the dotted lines. The regulation mileage is shown by the blue line, which keeps increasing whenever there is a change in energy storage power output, as shown in equation (2.2).

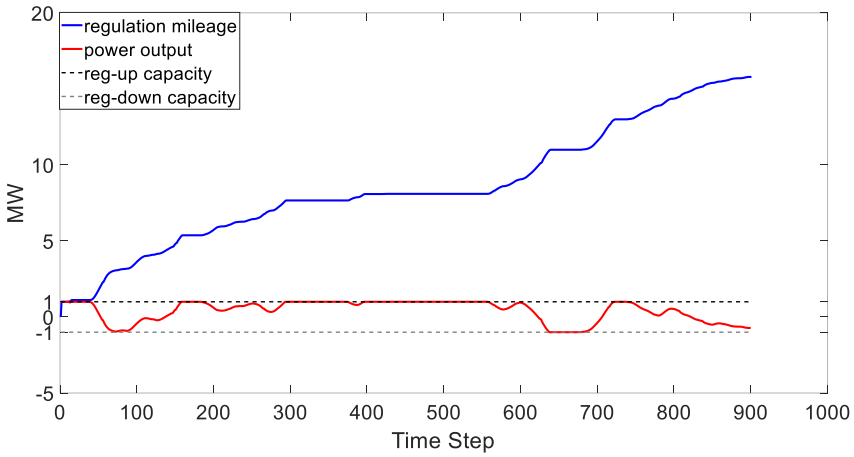

Figure 2. 7 An example of regulation capacity and mileage.

2.2 Modeling of ESS

This section is organized as follows. Sub-section 2.2.1 describes the modeling of ESS operation, which will be used in the whole dissertation. Sub-section 2.2.2 introduces lifetime estimation method of ESS.

2.2.1 ESS Operation Model

In this dissertation, we consider two kinds of ESS technologies-Lithium-ion battery and flywheel. These two technologies have the same operation, only different parameters. We assume that Li-ion battery or flywheel can ramp up or down to any power output within its rated power in milliseconds so that the instruction regulation signals can be followed accurately and immediately, unless the unit is fully charged or discharged. The storage charging and discharging process and constraints can be modeled as

$$E_t - E_{t-1} = \Delta t \eta_c P_t^{RegDown} - \Delta t \eta_d P_t^{RegUp} - \Delta t P_t^{SelfDisc} \quad (2.4)$$

$$0 \le P_t^{RegDown} \le P_{bid}^{reg} \quad (2.5)$$

$$0 \le -P_t^{RegUp} \le P_{bid}^{reg} \quad (2.6)$$

$$E^{Lowerlim} \le E_t \le E^{Upperlim} \quad (2.7)$$

where P_t^{RegUp} and $P_t^{RegDown}$ represent the regulation-up and regulation-down signals at time t, respectively; E_t is the energy level at time t; $E^{Upperlim}$ and $E^{Lowerlim}$ is the storage upper and lower energy limits, respectively; Δt is the duration of regulation signal; η_c and η_d represent storage charging and discharging efficiency, respectively; and $P_t^{SelfDisc}$ is the self-discharging rate.

2.2.2 ESS Lifetime Estimation

Both the capacity and power capability of batteries are incrementally degrading as they are being operated. The use of batteries is limited by its lifetime [29]. The chemistry of battery aging process is typically modeled with partial differential equations, which have good accuracy, but are highly nonlinear and complicated [30], [31]. Instead, the lifetime of a battery storage system can be estimated based on how many charging-discharging cycles it has completed at different depths of discharge (DOD), which is used to describe how deeply the battery is discharged. For example, if the battery have delivered 30% of its energy, here are 70% energy reserved, the DOD of this battery is 30%. Each battery should have a defined cycle life-the number of cycles for a given DOD, which is the number of discharge when the battery is discharged at the certain DOD rate until the battery's end of life [32]. As shown in figure 2.8, the battery cycle aging is highly nonlinear with respect to the cycle depth, which lead to shallow cycles cause much lower aging damage per MWh of energy throughput [33]. This phenomenon: smaller cycle depth results in a higher lifetime energy throughput is observed in most static electrochemical batteries [34]. Because a battery storage system providing regulation services will not run full cycles at a given DOD level, the Rain-flow method [35] is used to estimate battery lifetime depreciation. Note that the flywheel lifetime is not influenced by DOD, so its lifetime as a function of DOD (see the blue line in figure 2.8) is constant.

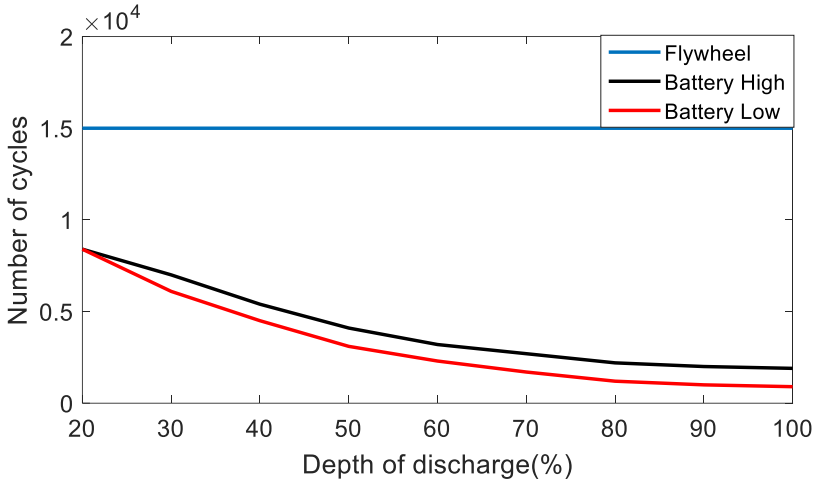

Figure 2. 8 Storage cycles over its life versus depth of discharge (DOD).

2.3 Cost-Benefit Study for ESS Providing Regulation Service

This section is organized as follows: Sub-section 2.3.1 introduces the energy storage benefit-cost model and performance criterion. Sub-section 2.3.2 analyzes the case studies. Sub-section 2.3.3 summarizes the conclusions and states the future work.

2.3.1 Modeling Methods

A. Energy storage benefit-cost model

We assume there is no start-up nor shut-down costs associated with energy storage operation when providing regulation services. The revenue R, and the cost C, can be calculated as

$$R = R_{mileage} + R_{capacity} \tag{2.8}$$

$$C = C_{install} + C_{O\&M} \tag{2.9}$$

where $R_{mileage}$ and $R_{capacity}$ represent the payments for regulation mileage and capacity respectively; $C_{install}$ and $C_{O\&M}$ represent the cost for installation and operation and maintenance, respectively. The parameters for the lithium-ion battery and flywheel used in this analysis are shown in Table 2.2 [36].

Table 2. 2 Storage characteristics.

ESS Technology	Lithium-ion battery	Flywheel
$\boldsymbol{\eta_c}$	0.85	0.95
$\boldsymbol{\eta_d}$	1	0.95
$\boldsymbol{P_t^{SelfDisc}}$	2-4% per month	2% per hour

Because the lifetime of battery varies when responding to different regulation signals or in different modes, annualized net benefits are calculated using the equivalent annual annuity approach (EAA). We first compute the net present value (NPV), followed by EAA so that the present value of the annuities is exactly equal to the project's NPV.

$$PV_{revenue} = \sum_{i=1}^{N} \frac{R(i)}{(1+r)^i} \tag{2.10}$$

$$PV_{cost} = \sum_{i=1}^{N} \frac{C(i)}{(1+r)^i} \tag{2.11}$$

$$NPV = PV_{revenue} - PV_{cost} \tag{2.12}$$

$$\text{EAA} = \frac{r \times NPV}{(1-(1+r)^{-N})} \tag{2.13}$$

where N is the estimated lifetime of energy storage, for simplicity, if estimated lifetime is not an integer, it will be round to the nearest greater integer, and r is the discount rate. In (2.10) and (2.11), R and C are annual values.

B. Performance criterion

To evaluate the regulation signal following accuracy, we define the response rate as

$$RR = \frac{n_{fulfilled}}{n_{total}} \times 100\% \tag{2.14}$$

where $n_{fulfilled}$ is the number of regulation signals fully followed by the storage unit and n_{total} is the total number of regulation signals. If the storage unit has enough energy for regulation-up or

enough energy space for regulation-down, the regulation signal is fully followed. Otherwise, the energy storage unit doesn't respond to the signal.

The remaining battery life after providing the regulation signal L_{remain}, can be estimated by the rain-flow method mentioned before. Thus, the aging ratio A, is

$$A = \frac{L_{default} - L_{remain}}{L_{default}} \times 100\% \quad (2.15)$$

2.3.2 Simulation Results

A. Simulation setup

The following assumptions are made when performing the simulation:

- For one-directional service, the battery/flywheel is fully charged when $t = 0$.
- For bi-directional service, the state of charge (SOC) of the battery/flywheel is 50% when $t = 0$.
- The battery/flywheel is always online (charging, discharging, or idling), so the start-up or shut-down costs are not considered.
- The default battery life is assumed to be 10 years, and the default flywheel lifetime is assumed to be 20 years.
- The rated power of the battery and flywheel is 1 MW and the energy capacity is 0.5MWh.
- Regulation signals are downloaded from the PJM and NYISO websites. The PJM regulation signal includes two parts: PJM RegD and PJM RegA. The NYISO regulation signal has not yet been divided between fast and slow units, so only one signal is used. Regulation signals and corresponding price data in 2017 are used to conduct the analysis.
- When calculating annualized costs and benefits, the annual discount rate is 10%.

B. Simulation results

As introduced in previous sections, regulation signals and the corresponding price data in our study were downloaded from PJM (i.e. RegD and RegA) and NY-ISO website. The data resolution is 2-second for PJM and 6-second for NY-ISO. The data was collected from January 1st to December 31st, 2017. Using the aforementioned parameters and simulation settings, we calculate the mileage and response rate of the Lithium-ion battery and flywheel when providing regulation services. The rain-flow algorithm is used to estimate the lifetime of the Lithium-ion battery storage system assuming that the designed lifetime of battery is 10 years.

Impact of using Different Regulation Signals

For this part of the analysis, we assume the service is provided by a Lithium-ion battery in bi-directional mode. The performance criterion and daily revenue is calculated assuming that DOD is at 50% at the beginning of each day and parameters of the battery are as listed in Table 2.1.

Figure 2.9 shows the daily revenue over the whole year. As the revenue is calculated from the regulation service price, the revenue will spike when regulation prices spike. The maximum revenue is $1970, the minimum revenue is $231, and the mean value is 542 $/day [37].

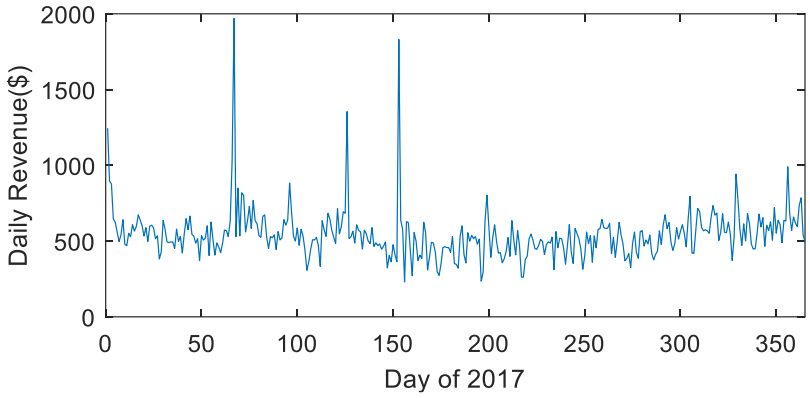

Figure 2. 9 Daily revenues for providing 2017 NYISO regulation signals.

Figure 2.10, 2.11, and 2.12 show the statistical spread in daily revenue, response rate, and aging cost, respectively, for the Lithium-ion battery. From the results, we have several observations. First, as shown in figure 2.10, revenue is the highest when providing RegD signals,

almost twice as much as the revenues received for other types of regulation signals. This result is due in part to PJM's higher market clearing prices for regulation mileage compared with NYISO. For example, in June 2017, the PJM mileage price was $2.9334/MW and $0.1868/MW in NYISO. Second, as shown in figure 2.10, for NYISO and PJM, the revenue is similar if PJM does not allow regulation signals to be separated into RegD and RegA signals. Third, as shown in figure 2.11, the response rates are the highest for the RegD signal, as it is designed to be energy-neutral and the lowest for the RegA signal, which is energy-biased because the energy-neutral RegD signal has been separated out. As can be seen in figure 2.11, NY-ISO and PJM signals are different, causing 10% response rate differences. Fourth, as shown in figure 2.12, when following RegD signals, the battery mileage and lifetime depreciation increase. This result shows that there is a tradeoff between providing the high value RegD signal and increased service cost.

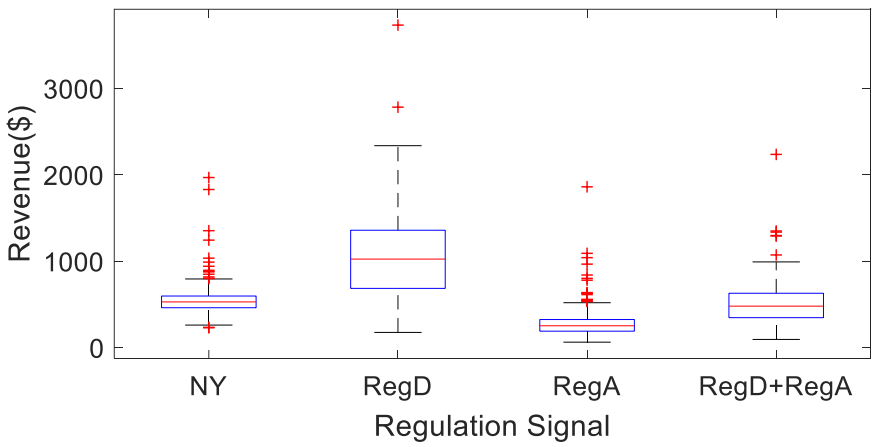

Figure 2. 10 Comparison of daily revenue across the year, associated with following different signals.

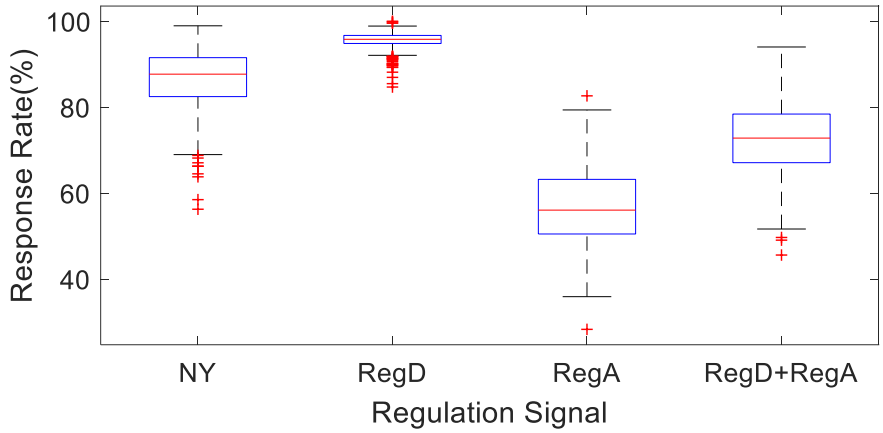

Figure 2. 11 Comparison of daily response rate.

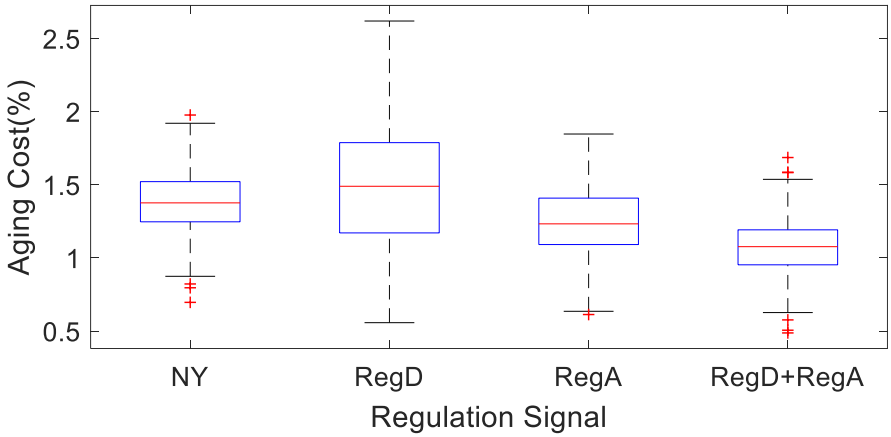

Figure 2. 12 Comparison of lifetime depreciation. Note that aging cost is the percentage of life reduction after one day of service.

Comparison of Different Technologies

Because RegD is designed to be a storage-friendly regulation signal, we use RegD to compare the performance of two different types of storage technologies: lithium-ion batteries and flywheels. Both 1-directional and 2-directional modes are considered. The power capacity of both devices are set at 1 MW and the energy capacity is 0.5 MWh. The initial energy for both devices is 0.25 MWh. Cost parameters of the lithium-ion battery and flywheel are listed in Table 2.3. We calculated the annual revenue received when providing ancillary services in 2017 and assume the same revenue can be received over the entire storage unit lifetime.

Table 2. 3 Storage cost parameters.

	Li-ion(0.5hr)	Li-ion(2hr)	Li-ion(4hr)	Flywheel
Current Cost ($/kWh)	1162	498	369	4541
2030 Cost ($/kWh)	532	228	200	4541
O&M($/kW·yr)	2	8	15	7

As shown in figure 2.13, the annual net benefit (i.e., profit) for both the battery and flywheel is positive when supplying RegD, indicating that for both 1-directional and 2-directional services, the operation is profitable. The net annual benefit of the 2-directional service is higher than that of the 1-directional service, due to the higher response rate and more mileage payments. The flywheel and Lithium-ion battery have similar performance. For one-directional service, the annual net benefit from the 0.5-hour Lithium-ion battery is $426/kWyr (2019 battery cost), compared with the flywheel net benefit of 307 $/kWyr. For bi-directional PJM RegD service, the annual net benefit of the 0.5-hour Lithium-ion battery is approximately $30/kWyr higher than the flywheel.

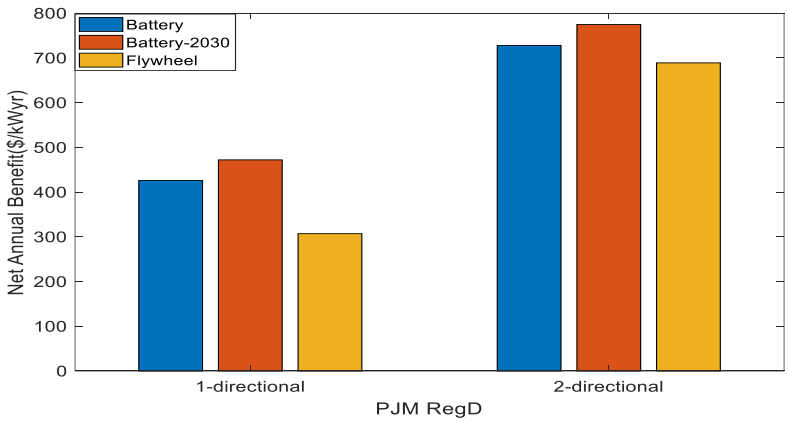

Figure 2. 13 Comparison of Lithium-ion and flywheel net benefit for 1-directional and 2-directional services.

We also compared the flywheel and Lithium-ion battery performance for the other types of regulation signals when providing 1-directional and 2-directional services. The results are summarized in Table 2.4.

Table 2. 4 Performance comparison when using different types of regulation signals and charging methods.

		PJM RegD		PJM RegA		NY-ISO	
		1-direction	2-direction	1-direction	2-direction	1-direction	2-direction
Battery	Annual net benefit ($/kW·yr)	426	728	81.0	65.4	201	310
	Response Rate (%)	49.4	95.0	34.8	55.7	48.1	85.5
	Estimate Lifetime (yrs)	4.72	3.89	5.93	4.23	5.28	3.99
Flywheel	Annual net benefit ($/kW·yr)	307	689	14.3	551	56	227
	Response Rate (%)	49.6	94.9	35.4	59.1	47.7	86.3
	Estimated Lifetime (yrs)	20	20	20	20	20	20

From the simulation results, the following two observations are made. First, if regulation signals are designed to be energy storage friendly, we can use energy storage to provide high-quality regulation services. As shown in Table 2.4, energy storage performance is best when supplying the PJM RegD signal. The response rate for both battery and flywheel are the highest when responding to PJM RegD signal. The PJM RegA is the most unfriendly to energy storage. The response rate of the battery supplying PJM RegA signal in bi-directional mode is only 55.7%, much smaller than that of supplying PJM RegD (95.0%) and NY-ISO (85.5%) signals. As mentioned before, RegD and RegA represent two distinct parts of the traditional regulation signal, similar to the single NY-ISO regulation signal. RegD is the part designed as energy-neutral, suitable for energy storage systems, while RegA is the remaining part, which has a large energy bias. If ranked by the friendliness to energy storage, we have RegD > NY-ISO > RegA, which is supported by the simulation results.

Second, battery and flywheel have similar technical performance in terms of response rate because both technologies respond fast and they have the same power and energy rating. Although

the Lithium-ion battery exhibits significant degradation, our model results indicate that it is still significantly more cost-effective than the flywheel.

Comparison of Different Battery Durations

Lastly, we compared the annual net benefit when using different battery sizes. Three Lithium-ion battery sizes are considered with 0.5 hour, 2 hour and 4 hour durations. The cost parameters are shown in Table 2.3. All three regulation signals are used and bi-directional service is considered. The initial energy is half of its maximum energy. As shown in figure 2.14, for all three markets, the longer the battery duration, the higher the net annual benefit. This result suggests that the incremental benefit associated with longer duration batteries exceeds the incremental cost. Furthermore, as shown in figure 2.14, running on shallow charging/discharging cycles causes less lifetime depreciation. For example, the service life of a 0.5 hour, 2-hour, 4-hour battery supplying the RegD signal are 3.8 years, 5.5 years and 10 years, respectively. It is important that a suitable energy size is selected to avoid the batteries being operated at low DOD for long durations.

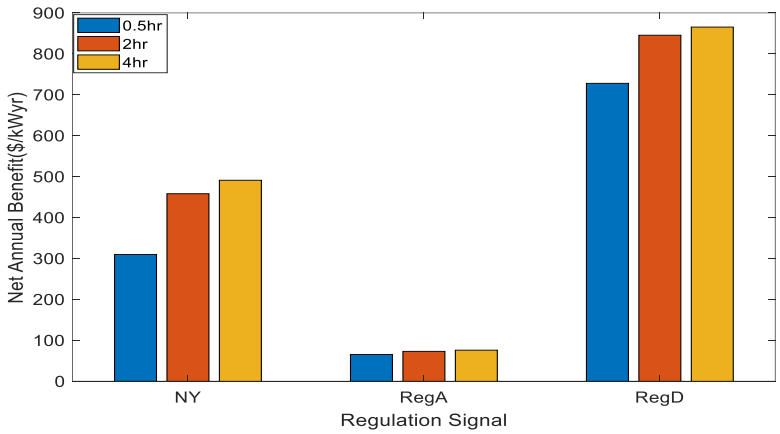

Figure 2. 14 Comparison of net annual benefits for different battery sizes.

2.3.3 Conclusions

In this section, a cost-benefit study is conducted to compare the performance and profitability of Lithium-ion batteries and flywheels providing grid regulation services. We used

regulation data collected by PJM and NY-ISO to benchmark the performance and the economics of using energy storage for providing regulation services.

It is worth pointing out that in this section the revenue is calculated using market clearing price, which is an idealized assumption when a market is saturated. Since the needed amount of regulation capacity is limited, this market can easily become saturated by too many price-taking participants, for example, operational evidence shows the PJM RegD market became saturated in 2016. Two main factors lead to the fast saturated of PJM RegD market: (1) Implementation of pay-for-performance market in PJM contributed to a 236MW increase of installed energy storage capacity in PJM from 2012 to 2016, with more than 90 percent of that capacity participating in the regulation market; (2) The rush of energy storage projects exposed some flaws in the design of PJM's frequency regulation market. For example, energy neutrality constraint led RegD resources to maintain power balance, regardless of the grid's reliability needs. PJM revised the market design and capped the share of RegD resources at 40 percent-down from an original cap of 62 percent-and established a 26.2 percent cap for RegD resources providing Regulation service during certain morning and evening "excursion hours" [38]. As we mentioned before, regulation market size is highly related to the penetration level of renewable energy, however it can be roughly estimated as 2-3% of system load. Before launching fast regulation signals, ISO/RTOs should find an optimal mix of fast regulation resources and slow regulation resources on the system.

To summarize, we draw the following conclusions from the results:

- To improve the ESS performance and best utilize its fast regulation capability, it is crucial to separate the regulation signal into a fast changing component, which should be energy-neutral and supplied by energy storage, and a slow moving component, which can be supplied by conventional units.

- To improve profitability and prolong battery lifetime, it is also important to operate battery cells at higher DODs. This can be achieved by either oversizing the battery storage system or pairing the battery storage system with another distributed energy resources.
- If providing 1-directional service is allowed, regulation services can be stacked with other services. This is especially important if the service providers only manage charging services such as EV charging facility owners. For example, when in charging mode, the service provider can provide regulation up service by stop charging.
- Regulation market size is small, usually 3~5% of the peak load, making the size of the regulation market of a regional grid approximately 200 to 300 MW. Therefore, the market size and value for ESS to provide fast regulation service may quickly diminish. It is then critical to plan ahead well the optimal share of the regulation service and announce it to the ESS developers to avoid over investment in the area.
- In grids with high penetration of renewables, microgrid operations are becoming attractive. Thus, using ESS to provide regulation and load following services inside a microgrid can become a new service option.
- Apart from regulation services, ESS can also provide ramping, frequency regulation, spinning and non-spinning reserves, which are relatively low-cost services. One can consider stacking those services whenever possible to increase the value proposition for ESS-based ancillary service.

2.4 Regulation Signal Design Using Empirical Mode Decomposition

This section presents an energy storage friendly regulation signal design method based on empirical mode decomposition (EMD). Conventional generators have slow response rate so they are less efficient and inaccurate when following fast changing regulation signals. Battery energy

storage systems (BESS) have very fast response rate and excellent ramping capability, making them ideal resources for providing fast regulation services. However, the limitation in energy storage capacity prevents the BESS from serving non-energy neutral signals for a prolonged duration. Existing BESS-friendly regulation signal designed is filter-based and does not guarantee the resultant fast changing signal is energy neutral. The advantage of using the EMD-based approach is that the regulation signal can be decomposed into a fast-changing part with zero local mean and a slow-changing part reflecting the overall trend. To demonstrate the improvement of the EMD-based approach on regulation signal design, we compare the regulation signals obtained using our method with the PJM RegA and RegD signals. Simulation results show that both the generator and BESS have better performance when responding to the EMD-based regulation signals compared with the filter-based RegA and RegD signals.

This section is organized as follows: Sub-section 2.4.1 introduces existing regulation signal design method and implementation. Sub-section 2.4.2 presents proposed regulation signal design algorithm based on empirical mode decomposition. Sub-section 2.4.3 analyzes the case studies. Sub-section 2.4.4 summarizes the conclusions and states the future work.

2.4.1 Modeling Methods

Traditionally, regulation services are provided by generators. In recent years, when the penetration level of wind and PV increases rapidly, both the ramp rate and capacity requirements of load balancing services increase significantly, causing an excess amount of large ramping actions on generator units. The wear-and-tear caused by fast and large ramping actions will shorten the lifespans of generator units. In addition, because traditional generation units are retiring or being displaced by renewable generation units, new resources for providing fast load following services are needed. The establishment of pay-for-performance market makes providing fast

regulation service a high-value ancillary service. Because of this, in the past few years, the share of BESS in the regulation markets increases rapidly.

Although BESSs can ramp up and down its power output quickly and can follow regulation signals accurately, they are energy limited so they are more suitable to serve energy neutral regulation signals [25]. Energy neutral means during a certain time period, the charging energy is roughly equal to the discharging energy. On the other hand, conventional generators have unlimited energy but limited ramping rates so they are suitable to provide slow-changing regulation signals. Considering the different characteristics of the two resources, it is necessary to redesign the regulation signals so that both resources can be operated more efficiently.

By the knowledge of authors, the topic-regulation signal design is not well studied in the literature. Currently, ISO-NE and PJM has implemented the separation of their regulation signal, however ISO-NE doesn't post the detailed design of how they separate the regulation signal. We believe that the method ISO-NE adapted should be very similar to the PJM one, because we found the following description in an ISO-NE document [39], "In a method similar to the Reg D implementation of PJM's AGC algorithm the ACE signal is then processed with a high-pass filter from which the output is a signal limited to the fleet energy storage regulation limits." On Jan.9, 2017, PJM began controlling regulation resources using conditional neutrality controller [40], the regulation signal has been separated as a fast-responding regulation D (RegD) signal and a slow-responding Regulation A (RegA) signal. As shown in figure 2.15, the conditional neutrality controller is a combination of proportional-integral-derivative controller (PID controller) and an internal feedback loop which maintains the SOC of ESS. The conditional neutrality controller does not forcibly converge the RegD signal back to zero within a fixed period of time. In this way,

RegD is providing short-term ACE control faster than the traditional RegA, with energy to be later balanced by the RegA resources when available to do so.

Typically, RegD signal is followed by ESS, the controller measures and records the accumulation of the injection and withdraw, which is equal to MWh depleted and charged from ESS. After the ACE deviation is stabilized, the RegA resources are additionally moved by a function of the RegD energy accumulation under the condition that there is extra available regulation capability to move the RegA resources. This mechanism maintains the SOC of ESS. In the implementation, the controller keeps checking the current value of ACE when determining this payback. If the ACE deviation is very large, the controller places priority on ACE control by tuning payback off until the regulation resources have ability.

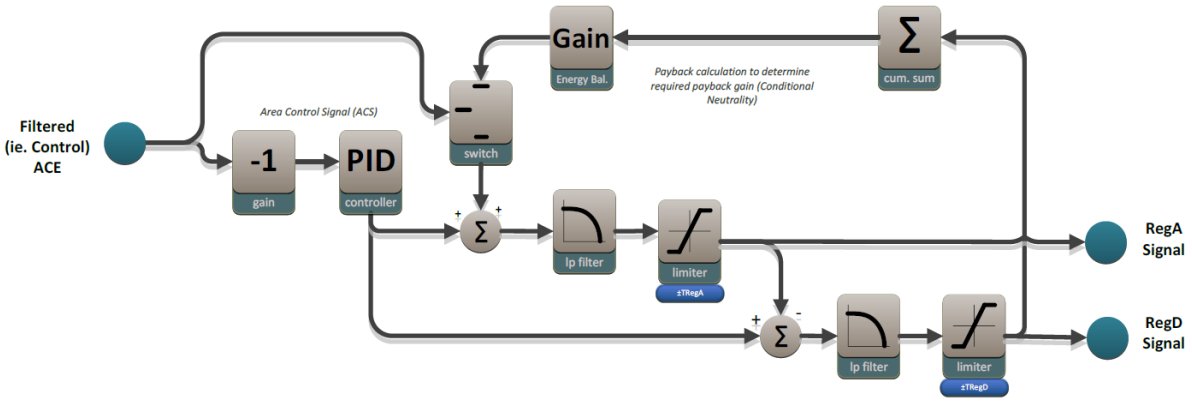

Figure 2. 15 High-level conditional neutrality controller [40].

Obviously, the method does not guarantee that the fast-changing signal will be an energy-neutral regulation signal. Therefore, the limitation in energy capacity prevents BESS from serving RegD signal for a prolonged duration. When responding to RegD signal, BESS can frequently be fully charged or discharged and lose its regulation capability. Therefore, in this section, we introduce a new regulation signal design method based on EMD [41]. EMD is a method for the analysis of non-stationary signals by decomposing a signal to several intrinsic mode functions

(IMF) and a residual. Each IMF must have zero local mean. If we generate fast-responding regulation signals as a combination of the IMFs, the zero local mean constraint of IMF will guarantee the fast-responding signal to be energy-neutral. Furthermore, using the EMD-based method does not require the design of complex parameters, making it easy to be implemented.

To illustrate the proposed method, we used a hybrid regulation resource (HRR) that consists of a BESS and a conventional generator to provide the PJM regulation signal. The results indicate the HRR has better performance when responding to the EMD-based regulation signals than the filter-based RegD and RegA signal.

2.4.2 EMD-Based Regulation Signal Design

A. Modeling of HRR

The BESS charging and discharging process and constraints have been modeled with equations (2.4)-(2.7). The model of conventional generator is shown in figure 2.16. This model consists of a delay block simulating the response delay to the setting signal, a first-order response model, a dead band element, an error part which models the respond deviations from the setting point, and a limiting block to make sure the output power not pass the generator regulation capacity [42].

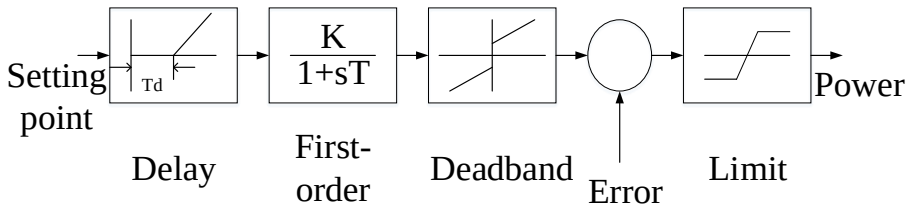

Figure 2. 16 Block diagram of the generator model.

B. Performance score

In part B of section 2.1.2, we introduce the general payment mechanism of pay-for-performance regulation market, illustrated with equation (2.3). In that section, only ESS, which

can have high response accuracy, is considered to provide regulation service. Thus we assume $\lambda = 1$, i.e. there is no payment penalization. However in this section, we consider conventional generator with limited ramping rate providing regulation service, the performance score should be evaluated.

The performance score (λ) is a value between 0 and 1, representing the response accuracy with respect to the regulation instructions. This score is used to decide resource's qualification to participate in regulation market and penalize the entire regulation payment. In PJM, performance score is the average of precision score, correlation score and delay score, which are all in the range between 0 to 1, for each 10 second over a five minute period [26]:

$$\lambda = \frac{1}{3}(PrecScore + CorrScore + DelayScore) \tag{2.16}$$

The precision score is calculated as a function of the difference in the energy provided versus the energy requested by the regulation signal while scaling for the number of samples for each 10 second interval. Error is calculated with respect to resource's regulation capacity:

$$Error = Avg\ of\ Abs\left|\frac{Response - Regulation\ Signal}{Hourly\ Average\ Regulation\ Signal}\right| \tag{2.17}$$

$$PrecScore = 1 - \frac{1}{n}\sum Abs(Error) \tag{2.18}$$

where n is the number of samples in the hour and the precision allows a 10 second latency for signal propagation delay for regulating resources.

Correlation score is the correlation coefficient between the regulation instruction and regulation response. Correlation score and delay score are calculated together, by finding the time delay under which the time-shifted regulation response has the highest coincident correlation and delay score.

$$CorrScore = r_{Signal,Response(\delta,\delta+5Min)} \tag{2.19}$$

$$DelayScore = Abs\left|\frac{\delta - 5Minutes}{5\ Minutes}\right| \quad (2.20)$$

where r is the statistical correlation function, which measures the degree of relationship between the two signals. Delay δ is defined at the point in time of the maximum correlation between the two signals, which is in the range of 0 to 5 minutes when calculating correlation score. Similar with PrecSocre calculation, 10 seconds latency is allowed. The 10 second interval that will determine CorrScore and DelayScore for each period is:

$$\max_{\delta=0\ to\ 5\ Min}(DelayScore + CorrScore) \quad (2.21)$$

PJM uses mileage ratio in its payment calculations. The formula for calculating the payments are as follows:

$$\text{Payment} = \lambda P_{bid}^{reg}(\rho_c + \frac{\text{M}}{M_{RegA}}\rho_M) \quad (2.22)$$

where ρ_c, ρ_M are capacity clearing price and mileage clearing price, respectively; M_{RegA} is the mileage of the regulation A signal.

C.EMD based regulation signal design

EMD is a method decomposes a signal into a sum of components, each component is called an IMF. IMFs have to satisfy two criterion: (1) the number of zero crossings can only differ at most one from the number of extrema; (2) the mean value of the envelope defined by the local maxima and the envelope defined by the local minima is zero. In our application, criterion 2 makes each IMF energy-neutral, which is suitable for fast-responding regulation signal design.

The second criterion can be formulated as follows:

$$\text{IMF}_\epsilon(t) = \frac{1}{\epsilon}\int_{t-\frac{\epsilon}{2}}^{t+\frac{\epsilon}{2}} IMF(r)dr = 0 \quad (2.23)$$

In practice, ϵ can be determined based on particular applications. Assume the original signal is $s(t)$ and residual is $r(t)$. At the beginning, $r(t) = s(t)$. First, an upper envelope $s_+(t)$

is constructed by fitting a line through all local maxima. Similarly, the lower envelope $s_{-}(t)$ can also be created. $s_{+}(t)$ and $s_{-}(t)$ together form a candidate for the time-varying amplitude of the IMF [43]. Candidate IMF can be calculated as follows:

$$\mathrm{IMF}_k(t) = r(t) - \frac{1}{2}(s_{+}(t) + s_{-}(t)) \tag{2.24}$$

If $IMF_k(t)$ doesn't match the two criterion, the procedure can be iterated with a new value of $r(t)$.If $IMF_k(t)$ satisfies the criterion, a new residual is computed:

$$r(t) = r(t) - \mathrm{IMF}_k(t) \tag{2.25}$$

with the updated residual, EMD process is repeated until the stop criteria is satisfied. There are several stop criteria, in this application, the maximum number of IMFs extracted criteria is utilized, which means decomposition stops when number of IMFs generated is equal to the predefined value. In this way, we guarantee the decomposition has the same structure.

The original regulation signal of PJM is unavailable. Before applying EMD decomposition, the original signal needs to be reconstructed from RegA and RegD. Assume the HRR participates in the regulation market. Let the bid-in power of the BESS be P_{ESS} and let BESS respond to the RegD signal. Let the bid-in power of the conventional generator be P_{Gen} and let the generator respond to the RegA signal. This is equivalent to say that the HRR system responds to a combined regulation signal of $P_{ESS} + P_{Gen}$. Thus, the regulation signal can be represented as

$$Reg(t) = \frac{P_{ESS}RegD(t)+P_{Gen}RegA(t)}{P_{ESS}+P_{Gen}} \tag{2.26}$$

This is because the RegD and RegA are within the range of [-1,1], so the reconstructed original Reg signal is also within the range of [-1,1].

Then, we apply the EMD algorithm to the $Reg(t)$ signal and generate fast-responding signal (EMD_fast) and slow-responding signal (EMD_slow). The EMD-based signal design process can be described as follows.

Table 2. 5 EMD based regulation signal design.

Algorithm 1 EMD based Regulation Signal Design	
1:	Residual r(t) = Reg(t), $I_1(t) = r(t)$
2:	i=1,k=1
3:	while k<Max number of IMF
4:	while I_i doesn't satisfy IMF cretirion
5:	$s_+(t)$ is the line through local maxima of I_i
6:	$s_-(t)$ is the line through local minima of I_i
7:	$I_i(t) = I_i(t) - \frac{1}{2}(s_+(t) + s_-(t))$
8:	i=i+1
9:	end
10:	$IMF_k(t) = I_i(t)$
11:	$r(t) = r(t) - IMF_k$
12	k=k+1
13:	end
14:	EMD_slow=r(t), EMD_fast=$\sum_{i=1}^{k} IMF_k(t)$

2.4.3 Case Study

A. Parameters of HRR system

Assume an HRR system consists of a 5-MW, 2.5-MWh Lithium-ion battery and a 5-MW hydro regulation capacity from a 400 MW hydro unit. The hydro unit needs to reserve 5MW capacity to provide regulation service. The rest of its capacity can be operated normally. The parameters of selected HRR is listed in Table 2.6 [36], [42]. The response delay time of hydro generator is 1 second, while the control error is in the range of [-0.3MW, 0.3MW] with the mean as zero.

Table 2. 6 HRR parameters.

	Li-ion Battery	**Hydro**
Maximum Capacity(MW)	5	400
Minimum Capacity(MW)	-5	100
Energy Capacity(MWh)	5	Unlimited
Charging efficiency (η_c)	0.95	N/A
Discharging efficiency (η_d)	0.95	N/A
Self-discharging rate($P_t^{SelfDisc}$)	2-4% per month	N/A
Response Time	<1 sec	60 sec time constant of first order model

B. Performance evaluation

To evaluate the signal following accuracy of Lithium-ion battery, we use the response rate defined as equation (2.14).

Mean absolute error (MAE) is used as the other metric for the regulation performance evaluation, which is defined as follows:

$$MAE = mean(\sum_{t=0}^{num} |P_{desired}(t) - P_{actual}(t)|) \quad (2.27)$$

where $P_{desired}$ is the desired power by instruction signal, P_{actual} is the actual power output by participating resources.

C. Impact of using different regulation signals

The regulation signal and corresponding clearing price of PJM in 2017 are used to conduct the analysis [10], where the regulation signal is updated every 2 seconds. To make sure the decomposed signal have the same structure, the window length of original signal when applying

EMD algorithm is 1 day, i.e. $30 \times 60 \times 24 = 43200$ samples. One day regulation signal and its IMF components are shown in figure 2.17.

Based on the historical data analysis, the maximum number of IMFs is set as 7. The amplitude of all 7 IMFs oscillates over zero. Since each IMF has zero mean, the combination of IMFs also have a zero mean, which is ideal for fast-responding regulation signal. Also, as the index of IMF increases, the frequency decreases, i.e. the later the IMF is extracted, the smoother it is. This characteristics leads to the flexibility when designing the signal. Based on the characteristics of the slow unit in the HRR, we can decide which components constitute slow-responding regulation signal. For example, if the slow unit is a hydro generator, which has relatively fast response rates, one possible formation of the slow-responding regulation signal can be IMF6+IMF7+residual. If the slow unit is a combined cycle generator, which has relatively slow response rates, the corresponding regulation signal can include only the residual.

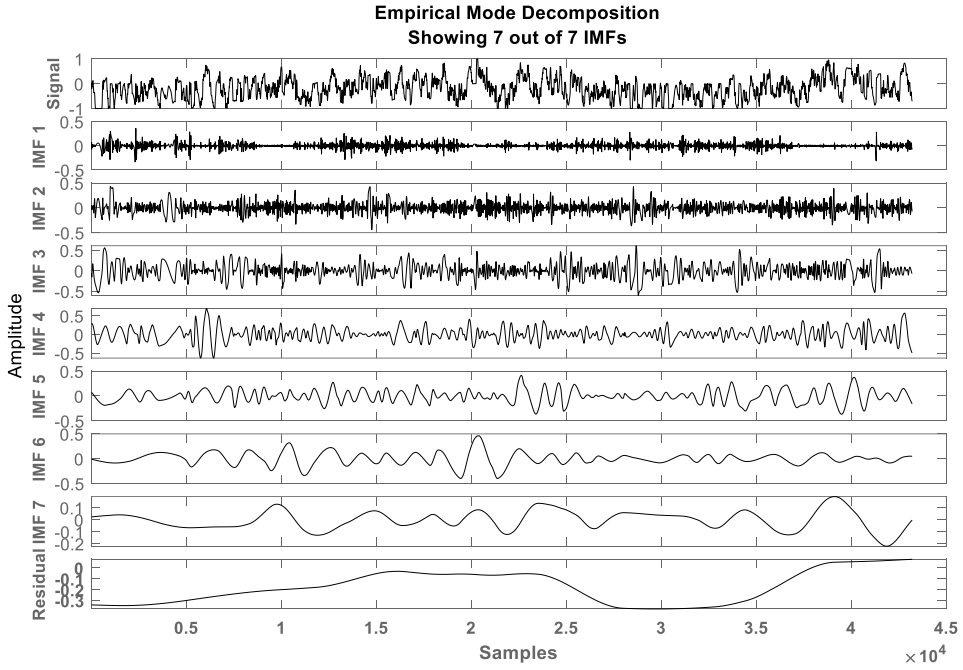

Figure 2. 17 One day regulation signal and its IMF components.

The performance of an Lithium-ion battery system when responding to the RegD and EMD_fast signals are listed in Table 2.7. The default battery lifetime is assumed to be 10 years.

As shown in Table 2.7, the battery responding to the EMD_fast signal has a higher response rate and a little longer estimated lifetime than those of responding to the RegD signal [43]. The change of SOC serving the EMD_fast signal is smaller than that of serving the RegD signal, which leads to a lower possibility of fully charged or depleted. In this example, the mean value of the hourly energy bias of the EMD_fast is 19.67 kWh, while that of the RegD signal is 161.64 kWh. Typically, a BESS running on shallow charging/discharging cycles causes less lifetime deprecation. Thus, providing the same amount of regulation energy, serving signal with lower energy bias results in a longer estimated lifetime.

Table 2. 7 Performance comparison of battery.

	Mileage (ΔMW/MW)	**Response Rate(%)**	**Lifetime (yrs)**
RegD	264880	95.54	2.97
EMD_fast	281420	96.66	3.04

The RegA and EMD_slow signals and the corresponding hydro generator responses are shown in figure 2.18.

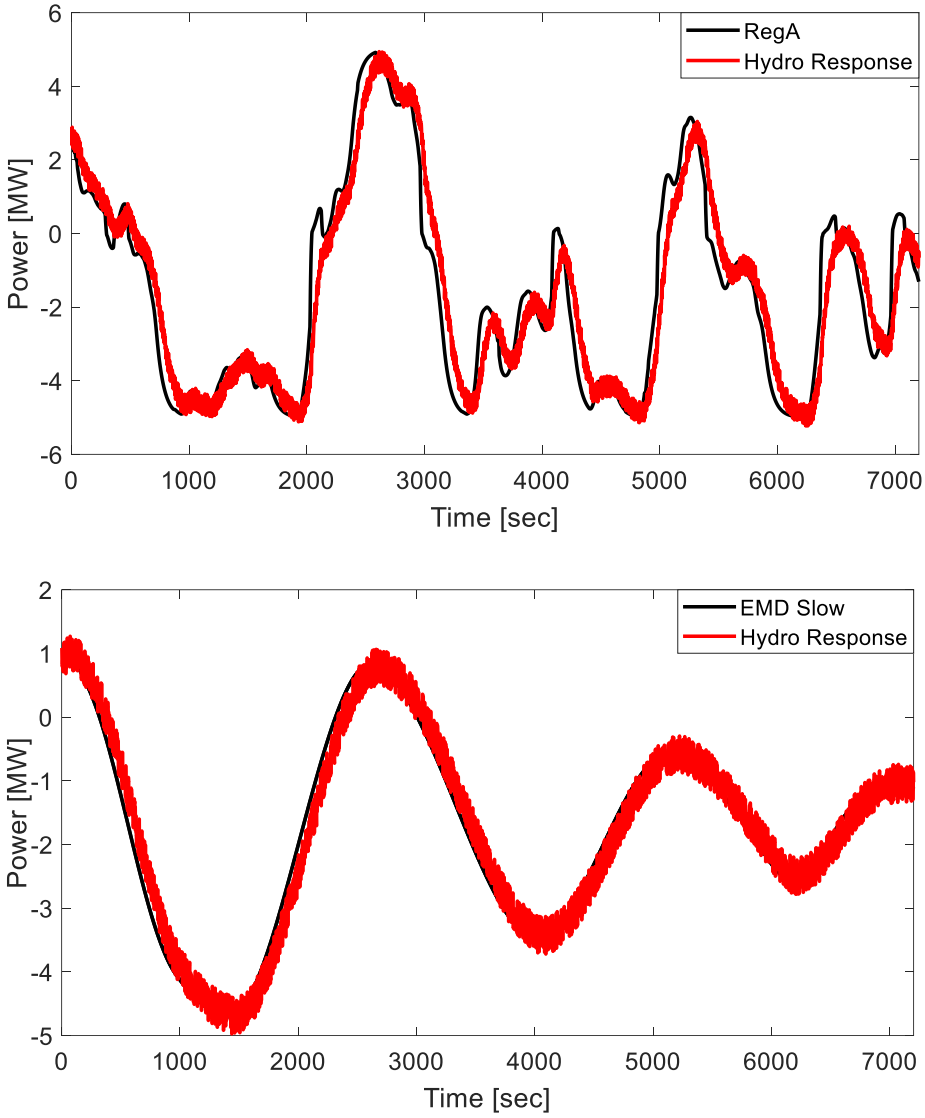

Figure 2. 18 Simulation results of hydro response: (a) Hydro generator responds to RegA signal, (b) Hydro generator responds to EMD_slow signal.

As shown in figure 2.18, EMD_slow and RegA have the same changing trend. However, EMD_slow is smoother, while RegA has more local maxima and minima. For example, corresponding to the obvious peak of RegA from 2000 to 3400 seconds, EMD_slow has a peak with longer duration (1500-4000 seconds) and lower peak value. Thus, the hydro generator has higher following accuracy serving EMD_slow than serving RegA. The MAE between the regulation service required by RegA and provided during the whole year is 0.4686 MW, while the

MAE of serving EMD_slow is 0.2317 MW. Therefore, the hydro generator has better performance when responding to the EMD_slow signal.

The Reg signal and HRR response are shown in figure 2.19. The response of HRR to EMD_slow and EMD_fast has higher following accuracy than that to RegA and RegD. There are two reasons for this phenomenon:1) EMD_slow is a smoother signal, thus hydro generator has better responding performance; 2) When responding to EMD_fast signal, the Lithium-ion battery system has shorter duration during which it will be fully charged/depleted so more regulation signals are supplied. Overall, the MAE between the regulation service required and provided when responding to existing PJM signal is 0.6366 MW, while the MAE when serving EMD based signal is only 0.4034 MW.

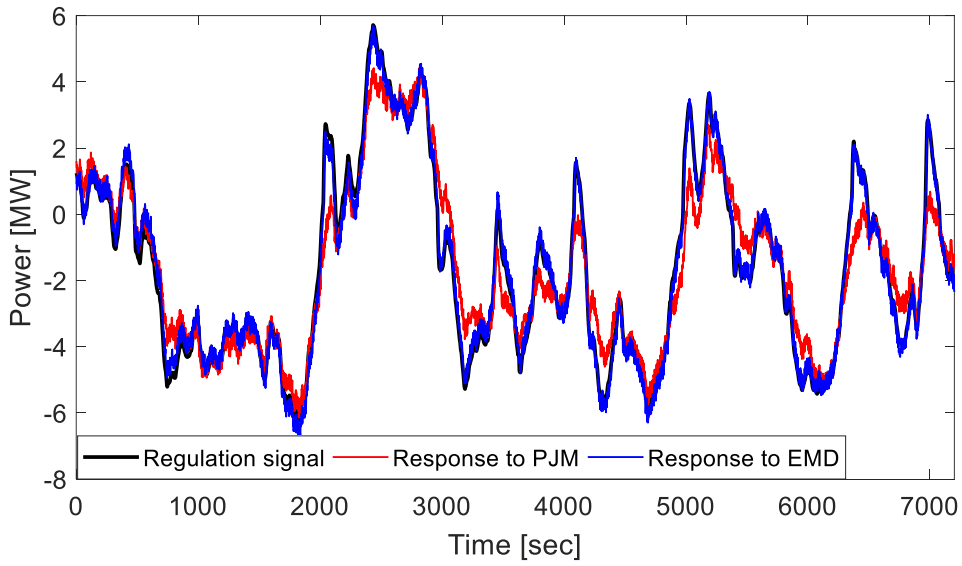

Figure 2. 19 Regulation signal required and the regulation service provided.

D. Cost-benefit study

In PJM, performance factor is used to test the qualification of resources participating in the regulation market, as well as penalize the regulation payment. Typically, the performance factor of conventional generator is smaller than that of the BESS. Assume that a hydro generator is

participating in the regulation market and it is responding to RegA with a regulation capacity of 5MW, the feasibility of investing a BESS to form an HRR is analyzed. The BESS is sized as 5MW and 2.5MWH. Based on [45], the Lithium-ion battery installment cost is assumed to be 1650 $/kWh and the operation and maintenance (O&M) cost is 10$/kWyr.

Table 2.8 compares the performance of three scenarios: a single hydro generator responding to the RegA signal, an HRR responding to the PJM signal, and an HRR responding to the EMD-based signal. When the HRR responds to the PJM signal, although the delay score keeps almost the same, both the correlation, precision, and performance scores will increase 0.149, 0.0852, and 0.0277, respectively. When the HRR responds to the EMD-based regulation signal, the correlation, precision, and performance score can be further improved by 0.0113, 0.0564, and 0.0296, respectively. A higher performance score will lead to a higher priority in the regulation resources pool and a higher probability to be selected to provide the regulation service. What's more, higher performance score will result in a higher revenue when providing the same amount of service.

Table 2. 8 Performance comparison.

	RegA	**PJM**	**EMD**
Performance Score	0.8445	0.8722	0.9018
Delay Score	0.8935	0.8925	0.8989
Correlation Score	0.8058	0.8207	0.8320
Precision Score	0.8331	0.9183	0.9747

The lifetime of battery when responding to the EMD_fast signal is 3.04 yrs. We calculated the annual revenue received in 2017 and assume the same revenue can be received over the entire

BESS lifetime. The benefit in this case is calculated as the HRR revenue responding to the EMD signal minus the revenue of a single hydro generator responding to the RegA signal. The cost is the battery installation and O&M cost. After calculation, the investment of a BESS is profitable and the profit is 1.18×106 $ in NPV value.

2.4.4 Conclusions

In this section, we propose a new regulation signal design algorithm based on EMD. The proposed signal design algorithm can separate the regulation signal into IMFs and the residual signal such that all IMF signals will have zero local means. Using the redesign of the PJM regulation signal as an example, we demonstrate that the proposed method can successfully separate the regulation signal into a BESS-friendly, i.e. energy neutral, fast changing regulation signal and a generator-friendly slow changing regulation signal A cost-benefit study is also conducted to show that it is profitable to use a hybrid energy system consisting of a BESS and a conventional generator to provide regulation service.

Regarding the future work, the control algorithm for minimizing the BESS lifetime depreciation and the sizing consideration for the hybrid system will be studied on.

CHAPTER 3 MITIGATION OF POWER SYSTEM FORCED OSCILLATION

This chapter introduces the study on utilizing ESS to mitigate power system forced oscillation. First, the mechanisms of forced oscillation is presented. Then how to use ESS to damp forced oscillation is described. Finally, a forced oscillation source location algorithm is proposed.

3.1 Introduction

This section is organized as follows. Sub-section 3.1.1 introduces low frequency oscillation. Sub-section 3.1.2 illustrates the mechanism of forced oscillation.

3.1.1 Low Frequency Oscillation

Low frequency oscillations compromise the power quality, cause damage to system equipment, and could even lead to catastrophic balckouts [46]. In general, those oscillations can be classified into two categories: PDNO and FO. A PDNO is caused by short-lived disturbances. PDNO normally occurs in systems with weak or negative damping, because an oscillation excited by a short-lived disturbance cannot be damped in time. Examples of such disturbances include the control actions of a high-gain fast exciter, power variations on long transmission lines, or poorly tuned control settings [47],[48]. PDNO can be suppressed by tuning parameters of power system stabilizer (PSS) or intertie line controls [49]. Bonneville Power Administration (BPA) has establishied Dispatcher Standing Order 303 to reduce the amount of the tie-line flow when system inertia is dangerously low.

An FO is normally resonance excited by external periodic disturbances. Resonance is the tendency of a system to oscillate with greater amplitude at some frequencies than the others. An FO can happen in a well damped system at a frequency close or equal to the intrinsic system frequency [50]. Because periodic small disturbances can be amplified by resonance, as long as the periodic driving source exists, the oscillation will persist and propagate rapidly to the whole

system. On November 29, 2005, a 20MW oscillation in Alberta, Canada led to a sustained oscillation with amplitude as high as 200MW on the California-Oregon Inter-tie lines. Low frequency oscillation severely threatens the security and stability of large-scale interconnected power systems in real-time operations. Common FO sources include a malfunctioned PSS, mechanical oscillations in generator turbines, cyclic load changes, and etc. [51],[52]. Periodical power fluctuations in wind farm outputs caused by wind shear and tower shadow effects or vibrations of floating offshore wind turbines are also sources of FOs [53],[54]. Thus, FOs are anticipated to occur more often in high-wind-penetration grids. Because the FO is caused by resonance, as long as the FO source exists, the oscillation will persist. Therefore, to quench an FO, it is essential to locate and remove the FO source. Next, the mechanism of FO will be derived mathematically.

3.1.2 Mechanism of Forced Oscillation

Take the single-machine infinite-bus (SMIB) system as an example, here we assume the external disturbance injected on mechanical power of generator or load active power is periodic signal, defined as follows, respectively:

$$\Delta P_T = \Delta P_{Tm} \sin(\omega t) \tag{3.1}$$

$$\Delta P_l = \Delta P_{lm} \sin(\omega t) \tag{3.2}$$

where ΔP_{Tm} and ΔP_{lm} are amplitude of disturbance, ω is the angular frequency of periodic disturbance. The linearized motion equation of generator rotor is

$$\frac{\mathrm{T}_J}{\omega_0}\frac{d^2\Delta\delta}{dt^2} + \frac{K_D}{\omega_0}\frac{d\Delta\delta}{dt} + K_s\Delta\delta = \Delta P_T - \Delta P_e \tag{3.3}$$

where T_J is the generator inertia time constant; ω_0 is the system reference angular frequency with $f_0 = 60$ Hz. δ is the generator power angle, K_D is the generator damping factor, K_s is the generator synchronous torque coefficient, ΔP_e is generator electromagnetic power output, ΔP_T is

the generator mechanical power output.

When the generator is only disturbed by mechanical power of generator, i.e. $\Delta P_e = 0$, from equation (3.3) we can get:

$$\Delta\ddot{\delta} + 2\xi\omega_n\Delta\dot{\delta} + \omega_n^2\Delta\delta = \frac{\omega_0}{T_J}\Delta P_{Tm}\sin(\omega t) \tag{3.4}$$

where ω_n is the system natural angular frequency and ξ is the damping ratio:

$$\omega_n = \sqrt{\omega_0 K_s/T_J} \tag{3.5}$$

$$\xi = \frac{K_D}{(2\sqrt{\omega_0 K_s T_J})} \tag{3.6}$$

The solution of (3.4) consists of a general solutions and a particular solutions. The particular solution is expressed as

$$\Delta\delta(t) = B_T\sin(\omega t - \phi) \tag{3.7}$$

Then the amplitude of forced oscillation caused by the disturbance on mechanical power is as follows:

$$B_T = \frac{\frac{\omega_0}{T_J}\Delta P_{Tm}/K_s}{\sqrt{[1-(\omega/\omega_n)^2]^2+(2\xi\omega/\omega_n)^2}} \tag{3.8}$$

From (3.8), we can see that when $\omega_{FO} = \omega_n$, the periodical driving force ΔP_T has the same frequency as the natural frequency of the generator system. Thus, a resonance will occur and the magnitude of B_T will reach its maximum. Then, the oscillation in the power output of the generator will propagate to the rest of the grid. When such an FO happens, PMUs located at other buses will bear distinct sequential time series relationships correlated with the distance between the PMU location and the location of the FO source.

When the system is only disturbed by periodic disturbance at active power of load, i.e. $\Delta P_T = 0$. Under this condition, the disturbance is not directly acted on the rotor of generator. Instead, it causes the change of generator rotor speed by varying the active power output of

generator, which also leads to forced oscillation [55]. Here we assume $\Delta P_e = C\Delta P_l$, where C is the distribution factor of disturbance on load side, denotes how much influence of the disturbance is distributed to each generator, obviously $0 < C < 1$. The linearized rotor motion equation under this condition is as follows:

$$\Delta\ddot{\delta} + 2\xi\omega_n\Delta\dot{\delta} + \omega_n^2\Delta\delta = -C\frac{\omega_0}{\mathrm{T}_J}\Delta P_{lm}\sin(\omega t) \tag{3.9}$$

Thus the amplitude of forced oscillation caused by the disturbance on load side is:

$$B_l = \frac{-\mathrm{C}\frac{\omega_0}{\mathrm{T}_J}\Delta P_{lm}/K_s}{\sqrt{[1-(\omega/\omega_n)^2]^2+(2\xi\omega/\omega_n)^2}} \tag{3.10}$$

Similarly, when $\omega = \omega_n$, the amplitude B_l reaches its maximum value. Comparing equations (3.8) and (3.10), the amplitude of forced oscillation caused by the disturbance on generator side is bigger than that caused by the same amplitude of disturbance on load side. The analysis process of forced oscillation caused by disturbance on generator side and load side is similar. To simplify the problem, we only consider the disturbance on generator side, which has greater influence on the system.

3.2 Damp Forced Oscillation with ESS

As mentioned before, the most effective countermeasure against forced oscillation is to locate and then remove the external disturbance. However, both detecting the forced oscillation and locating the external disturbance needs time. During this period, ESS can be utilized to damp forced oscillation and ensure no damage occur in the whole system. A control strategy based on resonant controllers is adopted to modulate active and reactive power supplied by E-STATCOM and the effects of oscillation can be eliminated [19], which will be introduced briefly in this section.

A SMIB system with E-STATCOM is shown in figure 3.1, the disturbance is injected at the side of generator, and the forced oscillation propagating to the rest of the system represented

by an infinite bus through a transmission line. E-STATCOM is installed between the disturbed generator and the infinite bus. E_g and δ_g mean the amplitude and phase angle of voltage source, E_b is the voltage amplitude of the infinite bus with the phase angle as 0. X_d', X_t, X_L and X_b are the transient reactance of generator, the leakage reactance of transformer, equivalent reactance between transformer and E-STATCOM, and the reactance between E-STATCOM and the infinite bus, respectively.

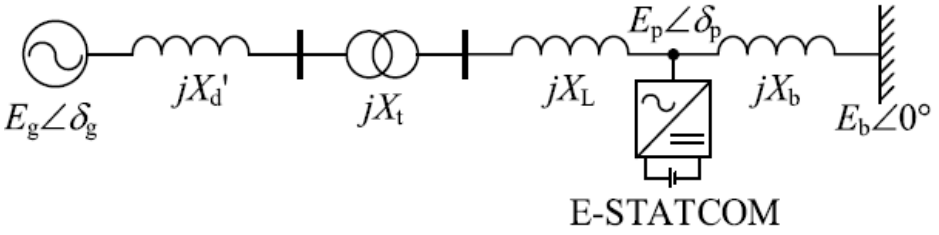

Figure 3. 1 SMIB system with E-STATCOM.

Figure 3.2 is the equivalent circuit of figure 3.1, where E-STATCOM is modeled as a current source supplying active and reactive power P_{inj}, Q_{inj}. P_g and Q_g are the active power and reactive power flowing from the generator to the bus connected with E-STATCOM. P_b and Q_b are the active and reactive power flowing to the infinite bus.

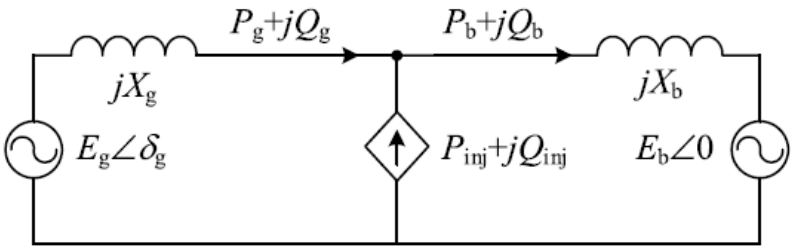

Figure 3. 2 Equivalent circuit of SMIB system with E-STATCOM [19].

Then the authors of [19] apply small-signal analysis to this SMIB with E-STATCOM system. The block diagram is obtained and showed in figure 3.3. δ_g, ω_g and ω_b are power angle,

rotor speed of the generator and base angle electrical speed, respectively. Δ represents the small perturbations in the corresponding variables.

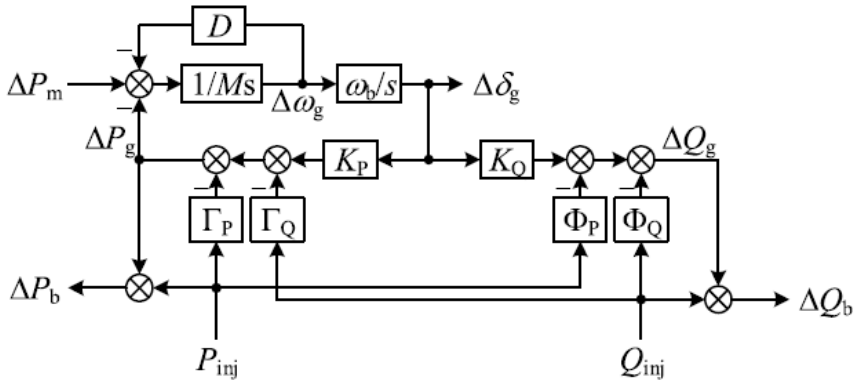

Figure 3. 3 Block diagram of SMIB system with E-STACOM.

ΔP_g can be expressed as:

$$\Delta P_g = K_P \Delta\delta_g - \Gamma_P P_{inj} - \Gamma_Q Q_{inj} \tag{3.11}$$

where K_P, Γ_P and Γ_Q are defined as follows:

$$K_P = \frac{\mathrm{E}_{g0}\mathrm{E}_{b0} cos\delta_{g0}}{X_g + X_b} \tag{3.12}$$

$$\Gamma_P = \frac{(1-a)^2 E_{g0}^2 + (1-a) a \mathrm{E}_{g0}\mathrm{E}_{b0} cos\delta_{g0}}{E_{p0}^2} \tag{3.13}$$

$$\Gamma_Q = \frac{(1-a) a \mathrm{E}_{g0}\mathrm{E}_{b0} sin\delta_{g0}}{E_{p0}^2} \tag{3.14}$$

The subscript 0 represents the value of the corresponding variable at steady state. Similarly, the expression of the reactive power ΔQ_g and K_Q, Φ_P, Φ_Q can be obtained:

$$\Delta Q_g = K_Q \Delta\delta_g - \Phi_P P_{inj} - \Phi_Q Q_{inj} \tag{3.15}$$

$$K_Q = \frac{\mathrm{E}_{g0}\mathrm{E}_{b0} sin\delta_{g0}}{X_g + X_b}(1 - 2a) \tag{3.16}$$

$$\Phi_P = -\frac{(1-a) a \mathrm{E}_{g0}\mathrm{E}_{b0} sin\delta_{g0}}{E_{p0}^2} \tag{3.17}$$

$$\Phi_Q = \frac{(1-a)^2 \mathrm{E}_{g0}^2 - a^2 E_{b0}^2}{2E_{p0}^2} - \frac{4a-3}{2} \tag{3.18}$$

The active and reactive power ΔP_b and ΔQ_b flowing to the infinite bus are expressed as

$$\Delta P_b = \Delta P_g + P_{inj} \tag{3.19}$$

$$\Delta Q_b = \Delta Q_g + Q_{inj} \tag{3.20}$$

To the rest of the system, ΔP_b and ΔQ_b can be seen as the disturbance sources. Thus, the control objective is to suppress the oscillations of ΔP_b and $\Delta Q_b$to 0 by tuning the power value of ESS, i.e. P_{inj} and Q_{inj}. The controller can be formulated as follows:

$$\mathrm{R(s)} = \frac{K_R s}{s^2 + \omega_c^2} \tag{3.21}$$

where ω_c is the central frequency of R(s) and K_R is the proportional coefficient. The differences between 0 and ΔP_b, ΔQ_b are used as the input signals of the two controllers, whose output values are power reference of E-STATCOM. The gain of R(s) at other frequencies are very small, enabling it to maintain the stability of the system. The proposed resonant controller are shown in figure 3.4.

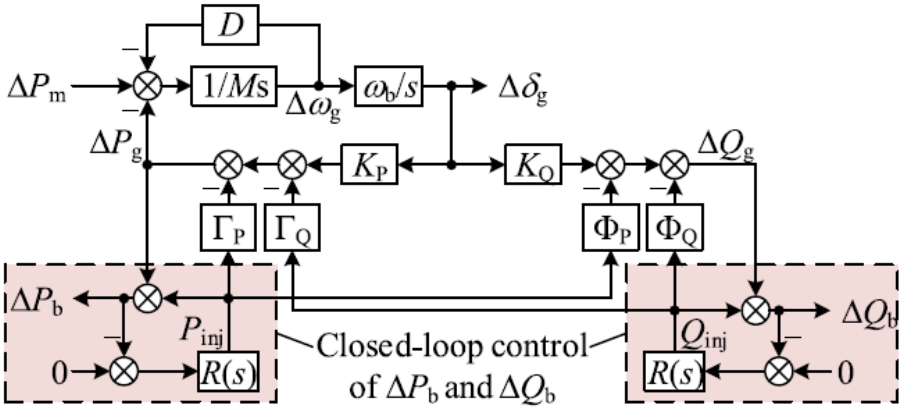

Figure 3. 4 Block diagram of suppression method [19].

For this suppression method of forced oscillation, there is not any assumption of the location of E-STATCOM, the operating condition or structure of the rest of the power system.

That means, no forced oscillations will pass through the bus connected with E-STATCOM to the rest of the system. It's worth noting the resonant controller works for frequency ω_c, oscillation is most serious when the frequency of the disturbance equals to system intrinsic frequency, so ω_c can be set as the intrinsic frequency which can be obtained by eigenvalue analysis.

Case studies using SMIB system shown in figure 3.1 are conducted to verify the proposed method. The system is rated as 13.8/230 kV, 200 MVA. The active power delivered by transmission line is 0.7 p.u. A 0.01 p.u. sinusoidal disturbance at 1.44 Hz is injected in the mechanical power output from 2s to 17s. The simulation results are shown in figure 3.5.

Without the proposed method, the oscillations of ΔP_b and ΔQ_b flowing out of the disturbed generator are 0.14 p.u. and 0.02 p.u., which amplify the disturbance by 14 and 2 times respectively. If the proposed method is implemented, ΔP_b and ΔQ_b are eliminated to 0 at steady state, this demonstrates the good suppression effect.

It's worth mentioning that the precondition of utilizing E-STATCOM to damp the forced oscillation effectively and efficiently is the location of disturbance source. Also, in a more complex meshed power grid, multiple equipment would be installed to better suppress forced oscillations, while the equipment near the disturbance source should be taken into effect to dampe the oscillation. What's more, the historical disturbance source should be taken into consideration when deciding where to place E-STATCOM. However, how to locate the FO source is not mentioned in [19]. Therefore a forced oscillation source location algorithm is proposed in the following section.

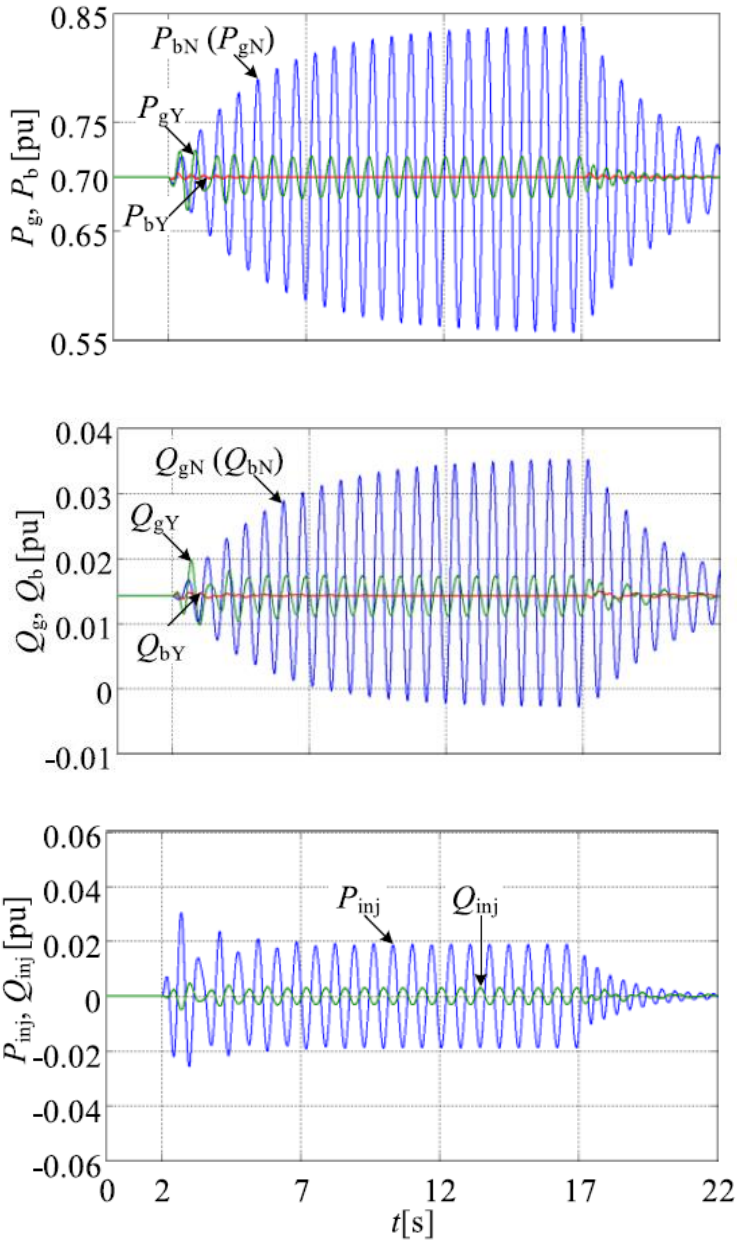

Figure 3. 5 Simulation results, where the subscripts Y and N denote the ones with and without the proposed method, respectively [19].

3.3 Forced Oscillation Source Location

Phasor Measurement Units (PMUs) have been widely installed in power transmission networks to provide fast-sampled and synchronized measurements. The transparency of power system has been enhanced with the fast-sampled and synchronized measurements. PMU data can

be used to detect, diagnose, and locate oscillations previously invisible to the conventional supervisory control and data acquisition (SCADA) systems [56]. Thus, how to deal with detrimental effects of forced oscillation is needed and will be the focus of this section.

In [57], Markham and Liu introduced a traveling wave based method for integrating PMU measurements at different places and identifying the generator with the earliest presence of oscillation as a source. The authors assume that the electric wave speed throughout the network is the same. This assumption may not hold in reality because electric wave speed varies between 50% to 80% speed of the light depending on the network parameters. In [58], [59], based on the transient energy function, the energy flow direction can be calculated to locate the forced oscillation source, which has already shown its practical performance in over 50 actual events. This energy-based method tracks the flow of effective transient energy, thus being model independent. However, it is hard to distinguish between a true source bus and a bus having a negative damping contribution. As illustrated in reference [60], the generator caused FO can be characterized as an effective current source in addition to its effective admittance. Prior knowledge of generator model structures is needed to implement this method. Authors of [61] locate the oscillation source by estimating the mode shape, which represents the relative magnitude and phasing of the oscillation throughout the system. Using tie-line power signal during oscillations, the real-time approximate entropy value in a continuous time interval, which is corresponding to the location of disturbance in power systems, can be calculated [62]. In [63], a machine learning approach is proposed. Measurement signals during forced oscillations are mapped to a multi-dimensional CELL, and decision tree is utilized to identify the characteristic parameters of the CELL corresponding to different oscillation sources.

Existing methods use data in (i.e. PMU measurements) the beginning phase of an FO. The inherent assumption of such method is once an FO occurs, it can be identified immediately. This assumption is not realistic in practice. Moreover, real-time ability is an important consideration when designing source location algorithms.

Existing methods only considered the accuracy for locating the FO source while the computational time requirements of those methods are often not given in the literature. Thus, whether or not a FO source locating algorithm can be executed in real-time is not known. In this paper, we propose a machine learning based method to locate the FO sources considering both the accuracy and computational time requirements.

The location problem is formulated as a multivariate time series (MTS) classification problem with each class membership corresponding to the location of the FO source. Sequential feature selection is used to identify the most informative PMU measurements for constructing MTS. Mahalanobis metrics are trained to represent the distance between the MTSs. To meet real-time identification needs, templates representing each class are constructed in offline training in order to improve the algorithm efficiency. Dynamic time warping (DTW) is applied so that MTS of different lengths and phases can be appropriately compared, relaxing the need to use data in the beginning phase of an oscillation.

This section is organized as follows: Sub-section 3.3.1 descripts the data preparation process. Sub-section 3.3.2 introduces proposed algorithm based on multivariate time series classification. Sub-section 3.3.3 presents results of numerical experiments.

3.3.1 Data Preparation

The MTS classification method uses two steps to locate the FO source: offline training and online identification. The data is generated through time domain simulation using *DSATools*^{TM} [64]. The following assumptions are made when generating the training data sets.

- This approach considers only single FO source caused by the disturbance injected at the generation side. The case for the multi-FO sources is ignored because its occurrence is rare. Thus, the number of FO source locations equals to the number of generator bus.
- The FO source is the power disturbance on a generation bus. This is because the periodic disturbance is often on a generator [58].
- To develop the algorithm, we assume that there are one PMU installed on each generator bus. Thus, there are N PMU installed for an N generator system.

As the first step, J typical system operation conditions are generated to emulate practical situations, i.e. load fluctuations. For a given operation condition j, we perturb one generator bus at a time until all N generators are perturbed. Thus, when the i^{th} generator bus is disturbed, the corresponding electromechanical transients recorded by all of the N PMU located at each generator bus will form a MTS matrix, $\boldsymbol{X}$.

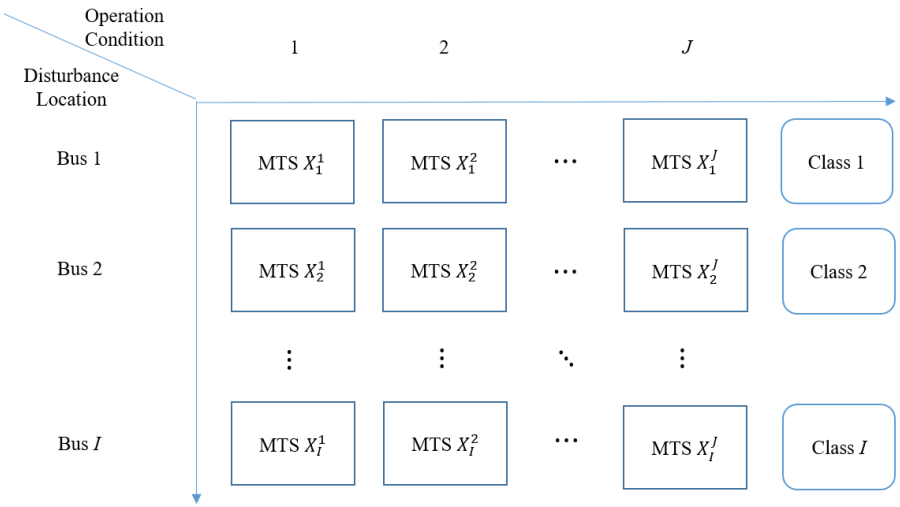

Figure 3. 6 Dataset Generation.

As shown in figure 3. 6, bunch of MTS are generated, each row denotes the location of forced oscillation source, each column denotes different operation conditions of power grid. The MTS matrices indexed as $\boldsymbol{X}_i^j(h,p)$. Subscript i denotes the location of generator being perturbed, i.e. oscillation source, since we assume oscillation source locates on generation side, the maximum value of i equals to N. In this work, we want to locate oscillation source, thus the MTS with the same subscript value are in the same class. Superscript j represents the different system operation conditions. Thus, we have

$$\mathbf{X}_i^j(h,p) = \begin{bmatrix} x_1(1) & x_2(1) & \cdots & x_p(1) \\ x_1(2) & x_2(2) & \cdots & x_p(2) \\ \vdots & \vdots & \ddots & \vdots \\ x_1(h) & x_2(h) & \cdots & x_p(h) \end{bmatrix}_{H\times P} \tag{3.22}$$

where h is the index of the number of sampling points and p is index of the PMU channels. Thus, each column represents the time series data of a selected PMU channel and each row is a snapshot of all selected PMU channels.

Because each PMU records several data channels (e.g. power angle, δ_i, real and reactive power, P_i and Q_i), a feature selection process is needed to determine the K most informative channels in order to construct the MTS. Thus, $P = N \times K$ and H is the total number of samples in the time series of the selected PMU channel.

3.3.2 Modeling Methods

A machine learning approach that utilizes PMU measurements to locate the source of forced oscillation geographically down to the substation level is proposed. It is assumed that at least one PMU measurement is available for each power plant, and the model of the power system is also available.

Figure 3.6 illustrates the proposed approach procedure. When forced oscillation occurs, the response of generators tends to be distinct for different oscillation source locations. Based on this intuition, dynamics of generators under various scenarios of forced oscillation source locations are generated through time domain simulation. Simulated PMU measurements of generators are utilized to construct signature multivariate time series. Mahalanobis distance is trained offline through metric learning. When a forced oscillation is detected, the same coefficients are measured and compared with the trained classifier to determine the source location of the oscillation. Dynamic time warping is applied to handle the out-of-sync between testing data sets and training data sets due to the oscillation detection delay.

A. Mahalanobis distance

In this work, Mahalanobis distance, a standard measure of the distance between two points in the multivariate space [65], is used to characterize the distance between two time series data sets. Let x and y be h^{th} row of two different MTS matrices $\mathbf{X}_{i_1}^{j_1}$ and $\mathbf{X}_{i_2}^{j_2}$:

$$x = \mathbf{X}_{i_1}^{j_1}(h, 1{:}P) \tag{3.23}$$

$$y = \mathbf{X}_{i_2}^{j_2}(h, 1{:}P) \tag{3.24}$$

Note that x and y represents the h^{th} data point of all P selected PMU channels when perturbing Generator i_1 and i_2 under operation condition j_1 and j_2, respectively.

Then, the Mahalanobis distance between x and y can be calculated as:

$$d_M(x, y) = (x - y)^T \boldsymbol{M}(x - y) \tag{3.25}$$

$$\boldsymbol{M} = \mathbf{U}\boldsymbol{\Sigma}\boldsymbol{U}^T \tag{3.26}$$

where $\boldsymbol{M}$ is the Mahalanobis matrix, a symmetry Positive Semi-Definite (PSD) matrix. The dimension of M is $N \times N$. If $\boldsymbol{M} = \boldsymbol{I}$, Mahalanobis distance degenerates to the standard Euclidean

distance. U is a unitary matrix that satisfies $\boldsymbol{U}\boldsymbol{U}^T = \boldsymbol{I}$. Σ is a diagonal matrix with singular values on the diagonal.

Thus, (3.25) can also be written as

$$d_M(x,y) = (x-y)^T \mathbf{U}\boldsymbol{\Sigma}\boldsymbol{U}^T(x-y)$$
$$= (\boldsymbol{U}^T x - \boldsymbol{U}^T y)^T \boldsymbol{\Sigma}(\boldsymbol{U}^T x - \boldsymbol{U}^T y) \quad (3.27)$$

where $\boldsymbol{U}$ is used to remove the correlation between variates so that the original space can be mapped into a new coordinate system and $\boldsymbol{\Sigma}$ servers as the weighting for the new variates.

The distance between $\mathbf{X}_{i_1}^{j_1}$ and $\mathbf{X}_{i_2}^{j_2}$ is defined as

$$\mathrm{D}_M\left(\mathbf{X}_{i_1}^{j_1}, \mathbf{X}_{i_2}^{j_2}\right) = \sum_{h=1}^{H} d_M\left(\mathbf{X}_{i_1}^{j_1}(h, 1\colon P), \mathbf{X}_{i_2}^{j_2}(h, 1\colon P)\right) \quad (3.28)$$

where $\mathbf{X}_{i_1}^{j_1}(h)$ and $\mathbf{X}_{i_2}^{j_2}(h)$ denotes the hth row in $\mathbf{X}_{i_1}^{j_1}$ and $\mathbf{X}_{i_2}^{j_2}$, respectively.

B. Metric learning

The Mahalanobis metric represents the relevance of two time series, which has the advantages over other traditional distance measures by eliminating the need to standardize the data [66]. Finding an optimal $\boldsymbol{M}$ to shorten the distance between the MTSs in the same class can improve the accuracy of member identification when locating the forced oscillation source. We use metric learning on the labeled training data to find an $\boldsymbol{M}$ that amplifies the influence of the location of the oscillation source while minimizing the influence of different system operation conditions. Therefore, for any two given sets of time series data in the MTS matrix, $\mathbf{X}_{i_1}^{j_1}$ and $\mathbf{X}_{i_2}^{j_2}$, the $\boldsymbol{M}$ learned should shorten the distance if $i_1 = i_2$, and lengthen the distance if $i_1 \neq i_2$.

Three common constraints: class label, pairwise label, and triplet label are used in metric learning. As discussed and proved in [67-70], triplet label is the weakest constraint and thus has the best performance. Regarding weakest constraint, triplet constraints can be derived from

pairwise constraints, but not vice versa. In this work, the triplet label is used to conduct metric learning.

As a first step, select a triplet label $\{\mathbf{X}_{i_1}^{j_1}, \mathbf{X}_{i_2}^{j_2}, \mathbf{X}_{i_3}^{j_3}\}$ so that $\mathbf{X}_{i_1}^{j_1}$ and $\mathbf{X}_{i_2}^{j_2}$ are in the same class (i.e., $i_1 = i_2, j_1 \neq j_2$) and $\mathbf{X}_{i_3}^{j_3}$ is in a different class (i.e. $i_3 \neq i_1$). Then, we define the constraint. Because the goal of metric learning is to find an appropriate matrix $\boldsymbol{M}$ so that distance between instances in the same class, i.e., $\mathrm{D}_M\left(\mathbf{X}_{i_1}^{j_1}, \mathbf{X}_{i_2}^{j_2}\right)$, should be closer than that in different classes, i.e., $\mathrm{D}_M\left(\mathbf{X}_{i_1}^{j_1}, \mathbf{X}_{3}^{j_3}\right)$ and $\mathrm{D}_M\left(\mathbf{X}_{i_2}^{j_2}, \mathbf{X}_{i_3}^{j_3}\right)$, the following constraint needs to be satisfied for all triplet constraints $\{\mathbf{X}_{i_1}^{j_1}, \mathbf{X}_{i_2}^{j_2}, \mathbf{X}_{i_3}^{j_3}\}$

$$\min\left(\mathrm{D}_M\left(\mathbf{X}_{i_1}^{j_1}, \mathbf{X}_{i_3}^{j_3}\right), \mathrm{D}_M\left(\mathbf{X}_{i_2}^{j_2}, \mathbf{X}_{i_3}^{j_3}\right)\right) - \mathrm{D}_M\left(\mathbf{X}_{i_1}^{j_1}, \mathbf{X}_{i_2}^{j_2}\right) > \rho \qquad (3.29)$$

where $\rho \geq 0$ represents the target margin. To simplify the description, in the following part we assume $\min\left(\mathrm{D}_M\left(\mathbf{X}_{i_1}^{j_1}, \mathbf{X}_{i_3}^{j_3}\right), \mathrm{D}_M\left(\mathbf{X}_{i_2}^{j_2}, \mathbf{X}_{i_3}^{j_3}\right)\right) = \mathrm{D}_M\left(\mathbf{X}_{i_1}^{j_1}, \mathbf{X}_{i_3}^{j_3}\right)$. If not, we swap the notation of the MTS.

In the training phase, as many triplet constraints as possible should be used to escape local minimums. However, because the number of triplets is the cubic of the number of the training samples, it is not practical to use all possible triplet combinations. Thus, a dynamic triplets building strategy based on the current learned $\boldsymbol{M}$ is proposed by Mei et al. in [71]. This method allows the most useful triplets to be chosen at the boundaries of different classes instead of randomly choosing triplets. For example, we can choose $\mathbf{X}_{i_2}^{j_2}$ to be the data point having the largest distance in the same class of $\mathbf{X}_{i_1}^{j_1}$, and $\mathbf{X}_{i_3}^{j_3}$ to be the one having the nearest distance with $\mathbf{X}_{i_1}^{j_1}$ in a different class.

The iterative process for updating $\boldsymbol{M}$ is explained as follows. First, select a triplet constraint as the input to the learning process. If (3.29) is satisfied, go to next iteration. Otherwise, update $\boldsymbol{M}$ to reduce the loss function $L(\boldsymbol{M})$, defined as

$$L(\boldsymbol{M}) = \rho + D_M\left(\mathbf{X}_{i_1}^{j_1}, \mathbf{X}_{i_2}^{j_2}\right) - D_M\left(\mathbf{X}_{i_1}^{j_1}, \mathbf{X}_{i_3}^{j_3}\right) \tag{3.30}$$

At each iteration, $\boldsymbol{M}$ is updated by minimizing the loss function. To guarantee the stability of the learning process, a regularization term that restricts the divergence of matrices is added to the metric learning model. Commonly used Bregman matrix divergence is defined as:

$$\begin{aligned}\mathrm{Div}(M_t, M_{t+1}) = \phi(M_t) - \phi(M_{t+1}) \\ -tr\left(\left(\nabla\phi(M_{t+1})\right)^T (M_t - M_{t+1})\right)\end{aligned} \tag{3.31}$$

where the function tr() stands for the trace of a matrix. Choose the differentiable function $\phi(M_t)$ as the Burg entropy of the eigenvalues:

$$\phi(M_t) = -\sum_i log\lambda_i = -\log\left(\det\left(M_t\right)\right) \tag{3.32}$$

The corresponding Bregman matrix divergence is called LogDet divergence [72], expressed as:

$$\mathrm{Div}(\boldsymbol{M}_t, \boldsymbol{M}_{t+1}) = \mathrm{tr}(\boldsymbol{M}_t\boldsymbol{M}_{t+1}^{-1}) - \log(\det(\boldsymbol{M}_t\boldsymbol{M}_{t+1}^{-1})) - \mathrm{N} \tag{3.33}$$

where N is the dimension of $\boldsymbol{M}$.

Thus, the $\boldsymbol{M}$ updating process [73] can be expressed as:

$$\boldsymbol{M}_{t+1} = \underset{M\succ 0}{\arg\min}\{Div(\boldsymbol{M}_t, \boldsymbol{M}) + \eta L(\boldsymbol{M})\} \tag{3.34}$$

where η is the parameter balancing the loss function $l(\boldsymbol{M})$ and the regularization term $Div(\boldsymbol{M}_t, \boldsymbol{M})$.

If η is too large, the learning process minimizes distances between the same class and maximizes the distance between different classes for each the triplet. This can result in an unstable

updating. If η is too small, the divergence between each iteration will be limited, leading to a slow learning process.

The objective function reaches its minimum when the gradient is zero. By setting the gradient of function $Div(\boldsymbol{M}_t, \boldsymbol{M}) + \eta l(\boldsymbol{M})$ as zero, we have

$$\boldsymbol{M}_{t+1} = (\boldsymbol{M}_t^{-1} + \eta(\boldsymbol{P}_t\boldsymbol{P}_t^T - \boldsymbol{Q}_t\boldsymbol{Q}_t^T))^{-1} \tag{3.35}$$

$$\boldsymbol{P}_t = \mathbf{X}_{i_1}^{j_1} - \mathbf{X}_{i_2}^{j_2} \tag{3.36}$$

$$\boldsymbol{Q}_t = \mathbf{X}_{i_1}^{j_1} - \mathbf{X}_{i_3}^{j_3} \tag{3.37}$$

where $\boldsymbol{P}_t$ denotes the difference between instances in the same class and $\boldsymbol{Q}_t$ denotes the difference between instances in the different class. To reduce the computation burden of matrix inverse, the standard Woodbury matrix identity introduced is used to solve (3.35) as follows:

$$(\mathbf{A} + \mathbf{UCV})^{-1} = \boldsymbol{A}^{-1} - \boldsymbol{A}^{-1}\boldsymbol{U}(\boldsymbol{C}^{-1} + \boldsymbol{V}\boldsymbol{A}^{-1}\boldsymbol{U})^{-1}\boldsymbol{V}\boldsymbol{A}^{-1} \tag{3.38}$$

Let $\boldsymbol{\Omega}_t$=$(\boldsymbol{M}_t^{-1} + \eta\boldsymbol{P}_t\boldsymbol{P}_t^T)^{-1}$ and apply the Woodbury matrix identity twice, the iterative expression of $\boldsymbol{M}_{t+1}$ is expressed as:

$$\begin{cases} \boldsymbol{\Omega}_t = \boldsymbol{M}_t - \eta\boldsymbol{M}_t\boldsymbol{P}_t(\boldsymbol{I} + \eta\boldsymbol{P}_t^T\boldsymbol{M}_t\boldsymbol{P}_t)^{-1}\boldsymbol{P}_t^T\boldsymbol{M}_t \\ \boldsymbol{M}_{t+1} = \boldsymbol{\Omega}_t + \eta\boldsymbol{\Omega}_t\boldsymbol{Q}_t(\boldsymbol{I} - \eta\boldsymbol{Q}_t^T\boldsymbol{\Omega}_t\boldsymbol{Q}_t)^{-1}\boldsymbol{Q}_t^T\boldsymbol{\Omega}_t \end{cases} \tag{3.39}$$

To ensure $\boldsymbol{M}$ is a PSD matrix, we require

$$\begin{cases} \eta(\boldsymbol{P}_t\boldsymbol{P}_t^T - \boldsymbol{Q}_t\boldsymbol{Q}_t^T) + \boldsymbol{M}_t^{-1} \geq 0 \\ \eta \geq 0 \end{cases} \tag{3.40}$$

This is a standard linear matrix inequalities (LMI). If the result of (3.40) is $\bar{\eta}$, then $\eta \in [0, \bar{\eta}]$ ensures that the updated $\boldsymbol{M}_{t+1}$ is a PSD matrix. Thus, the LMI is solved first to find the feasible range of η.

The algorithm runs cycle by cycle. In each cycle, select I_1 triplet constraints, where I_1 equals to the number of training samples, i.e. $I_1 = N \times J$. Thus, there are I_1 iterations in each cycle. Then, calculate the change of the total loss function L_k, where k is the index of cycle.

Two stop criterions are used: when $\left|\frac{L_k - L_{k-1}}{L_{k-1}}\right|$ is smaller than a predefined threshold, ϵ, or when the maximum number of cycles I_2 is met. Note that there is a tradeoff between the execution time and accuracy when selecting I_2. Although the Mahalanobis matrix learning process is the most computation-intensive step, it can be executed offline.

The Mahalanobis matrix learning process can be summarized as follows:

Table 3. 1 Mahalanobis matrix training algorithm

Algorithm 1 Mahalanobis Matrix Learning
Initialize Mahalanobis matrix as identity matrix
$k = 1, i = 1$
while $k < I_2$
while $i < I_1$
Select the most useful triplet constraint according to [71]
Calculate Mahalanobis distance using (3.28)
If (15) violated
Then update Mahalanobis matrix using (3.39)
$i = i + 1$
end
Calculate total loss function $L_k = \sum_i l_k(i)$
If $\left\|\text{abs}\left(\frac{L_k - L_{k-1}}{L_{k-1}}\right)\right\|$ <threshold, break
$i = 1, k = k + 1$
end

When forced oscillation occurs, PMU measurements are utilized to generate MTS with unknown class membership. With the learned Mahalanobis matrix, the distance between unknown MTS and the instances in training data sets can be calculated. The unknown object will be assigned to the most common class among its *k* nearest neighbors.

C. Dynamic Time Warping

In the offline training phase, all the training samples are generated through time domain simulation, and the beginning and ending time points are known. However, in real practice, it is unreasonable to assume the beginning and ending time can be identified accurately. As for this

oscillation source location problem, detection of the very beginning of the oscillation event is not guaranteed. Define *d* as the time needed for oscillation detection. The training data set begins right at the forced oscillation is incurred. While the testing data set begins at *d* seconds later than the forced oscillation occurs. Thus, the similarity of time series with different lengths and phases needs to be measured. Dynamic time warping (DTW) is an algorithm which can measure the similarity between out-of-sync time series by calculating an optimal warp path and mapping the two time series in one-to-one correspondence [74].

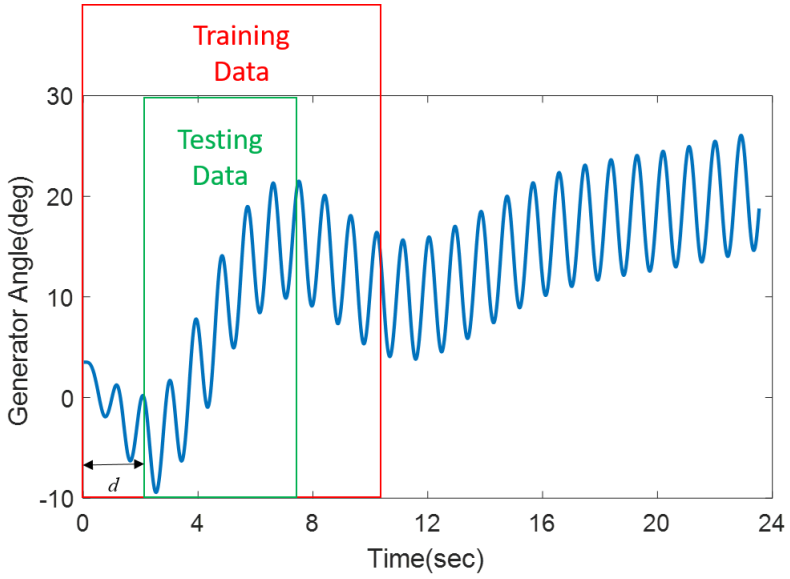

Figure 3. 7 Training and testing data set illustration.

Given two univariate time series $\mathrm{x}(i), i = 1,2, \dots, m$ and $\mathrm{y}(j), j = 1,2, \dots, n$. The optimal warp path W is the correspondence relationship, expressed as

$$\mathrm{W} = \begin{pmatrix} w_x(k) \\ w_y(k) \end{pmatrix}, k = 1,2, \dots, s \tag{3.41}$$

where $w_x(k) \in [1, m]$ represents an index of sequence $\mathrm{x}(i)$, $w_y(k) \in [1, n]$ represents an index of sequence $\mathrm{y}(j)$, s is the length of optimal warp path W, which should be in the range of $[\max(m, n), \ m + n]$. $\left(w_x(k), w_y(k)\right)'$ indicates the $w_x(k)^{th}$ element of sequence $\mathrm{x}(i)$ corresponds to the $w_y(k)^{th}$ element in sequence $\mathrm{y}(j)$.

To reduce the number of paths during the search, a valid warping path should satisfy two constraints [74]: (1) All indices of each time series are used in the warp path; (2) The warp path should be continuous and monotonically increasing. The conditions can be expressed as follows.

$$\begin{cases} W(1) = (1,1)' \\ W(s) = (m,n)' \\ w(k) \le w(k+1) \le w(k)+1 \end{cases} \tag{3.42}$$

Thus, $W(k+1)$ can only be selected from $\big(w_x(k), w_y(k+1)\big)'$, $\big(w_x(k+1), w_y(k)\big)'$ and $\big(w_x(k+1), w_y(k+1)\big)'$.

Traditional DTW works for univariate time series and the distance is measured by Euclidean distance. To extend DTW to MTS, each point of time series $\mathrm{x}(i), \mathrm{y}(j)$ changes from one singular value to a row vector. Then the Mahalanobis distance is applied to measure the distance between vectors using equation (11). The optimal warp path can be calculated through dynamic programming. Assume a distance matrix D with dimension equals to $m \times n$ is constructed, $\mathrm{d}_M(\mathrm{x}(i), \mathrm{y}(j))$ is the Mahalanobis distance between the i^{th} row vector of x and the j^{th} row vector of y. The calculation process of optimal warp path can be expressed as:

$$\boldsymbol{D}(\mathrm{i},\mathrm{j}) = \mathrm{d}_M(\mathrm{x(i)},\mathrm{y(j)}) + \min\begin{cases} \boldsymbol{D}(\mathrm{i}-1,\mathrm{j}-1) \\ \mathbf{D}(\mathrm{i}-1,\mathrm{j}) \\ \mathbf{D}(\mathrm{i},\mathrm{j}-1) \end{cases} \tag{3.43}$$

where $\boldsymbol{D}(1,1) = \mathrm{d}_M(\mathrm{x}(1),\mathrm{y}(1))$. The optimal warp path and corresponding distance can be obtained by computing all the elements in $\boldsymbol{D}$ matrix.

With the obtained optimal warp path W, the optimal alignment between two given MTS $\boldsymbol{X}$ and $\boldsymbol{Y}$ is defined. Thus, two new MTS with the same dimension $\widetilde{\boldsymbol{X}}$ and $\widetilde{\boldsymbol{Y}}$ can be generated, where

$$\begin{cases} \widetilde{\boldsymbol{X}}(k) = \boldsymbol{X}(w_x(k)) \\ \widetilde{\boldsymbol{Y}}(k) = \boldsymbol{Y}(w_y(k)) \end{cases} \tag{3.44}$$

The two new MTS have one-to-one correspondence, thus the distance between the two original MTS X and Y can be written as

$$\mathrm{D}(\mathbf{X},\mathbf{Y}) = \sum_{k=1}^{s} \mathrm{d}_M(\widetilde{\boldsymbol{X}}(k),\widetilde{\boldsymbol{Y}}(k)) \qquad (3.45)$$

Optimized warping path between two given time series is shown in figure 3.8.The dots denote the correspondence relationship between these two time series.

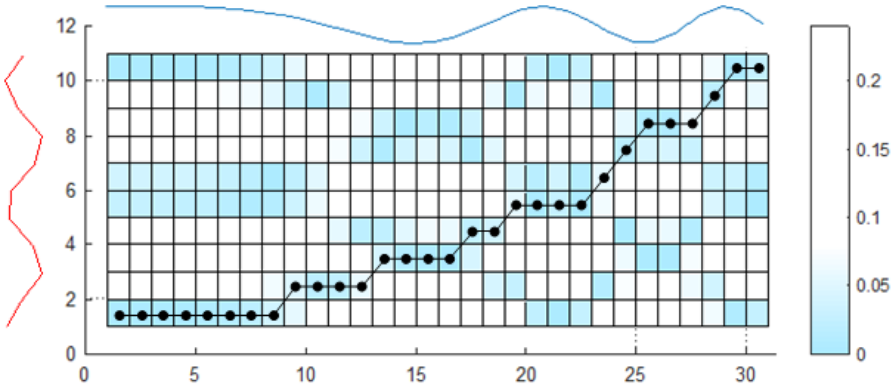

Figure 3. 8 An optimal warping path.

Now the distance between out-of-sync MTS is measured correctly. K-nearest neighbors algorithm (k-NN) is used for classification. The input of k-NN is the multivariate time series constructed by PMU measurements of generator rotor angle and active power; the output is a class membership. An object is classified by a majority vote of its neighbors, with the object being assigned to the class most common among its k nearest neighbors.

3.3.3 Numerical Experiments

In this section, numerical results of the proposal method are presented. The PMU measurement data sets used in case studies are generated by time-domain simulations using DSATools^{TM}. The sampling rate is 25Hz.

A sinusoidal signal served as the forced oscillation disturbance is injected into excitation systems. Rotor angle and active power of each generator serve as features. For training data sets,

the time series begins at 0s and ends at 15s, while for testing data sets, there is a delay d corresponding to the time needed for oscillation detection. Therefore, the testing time series starts d seconds later than the beginning of the oscillation and the window size of time is 5 seconds. The constructed multivariate time series is the same as (3.22), where p equals to two times the number of generators in the power grid, h equals to 25×15=375 for training sequences, and 25×5=125 for the testing sequence.

In all of the test system, all non-source generators are modeled as second order classical machines with damping factor D=4. The source generator is modeled as sixth order equations with an excitation system shown as figure 3.9, while the damping factor D=0.

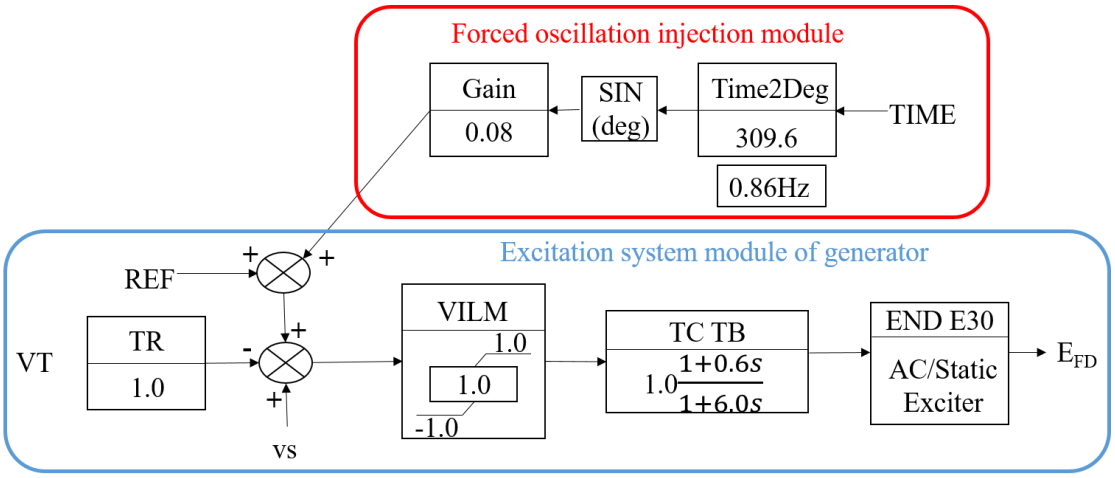

Figure 3. 9 Excitation system of source generator.

A. Four-machine two-area model

The detailed model parameters can be found in [13]. All generators are in a second-order model, while the load is in a constant impedance model. With the SSAT software, a detailed modal analysis on the system is conducted. The analysis results show that all natural modes have reasonably good damping and the system has a natural mode at $f_0 = 0.6208Hz$.

A sinusoidal signal $\Delta ref = k \times \sin(2\pi ft)$ emulating the oscillation disturbance is added to the reference signal of excitation systems, where $k = 0.03$. The oscillation begins at $t = 0s$. For each instance, only one of the generators is injected with the oscillation disturbance. To generate enough number of valid samples, the system load varies randomly between 90 percent and 110 percent of the original load. PSAT is applied to solve the power flow equations and the infeasible load conditions are removed. In reality, system parameters are time-varying and random, which leads to the discrepancy between the model and the real system. What's more, the frequency of oscillation source can cause resonance fluctuates within a specific range. To emulate practical situation, the damping factor of each generator which influences the low-frequency oscillation most is chosen randomly in [0, 4]. The frequency of oscillation source f fluctuates in the range of 90 percent to 110 percent of f_0.

Since only one of the generators acting as the oscillation source, there are four scenarios in total. Now the oscillation source locating problem converts to a multiclass classification problem. Following rules mentioned above, 800 samples (200 samples for each scenario) are generated. The ratio of training data sets and testing data sets is 1:1. To make the simulation more practical, Gaussian White Noise with the signal-to-noise ratio as 13dB is superimposed to the simulated PMU measurements. Assume the low-frequency oscillation can be detected in 3 seconds, so the testing time series begins at $d = 3s$. The dimension of training and testing multivariate time series is 375-by-8, 125-by-8 respectively. In the metric learning process, dynamic triplet constraint building strategy is applied to select triplet constraints. With the obtained Mahalanobis matrix, the distance between training samples and testing samples can be calculated. After that, k-nearest neighbor classification is applied to select the label of the nearest trained classifier as the category of the test sample with $k = 1$.

Table 3.2 presents the accuracy of oscillation source location. According to Table 3.2, the accuracy of all four situations is 100%， which indicates the effectiveness of the proposed approach.

Table 3. 2 Performance test of oscillation source identification for four-machine two-area model.

Generator with disturbance	Correct	Error	Accuracy/%
G_1	100	0	100
G_2	100	0	100
G_3	100	0	100
G_4	100	0	100

B. IEEE 39-bus system

The detailed model parameters can be found in [75]. Generators are in a fourth-order model, while the constant impedance load model is adopted. Based on the detailed modal analysis of the system, a natural mode with the frequency at $f_0 = 1.3217Hz$ exists.

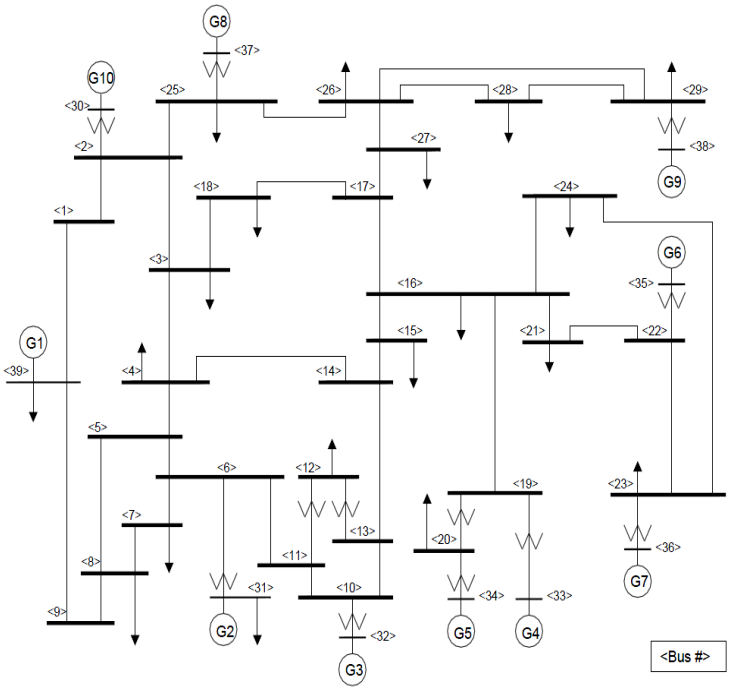

Figure 3. 10 IEEE 39-bus system.

Similar to the four-machine two-area case, a sinusoidal signal $\Delta ref = k \times \sin(2\pi ft)$ with $k = 0.6$ is added to the reference signal of excitation systems. Since each time only one generator acting as the forced oscillation source, there are ten scenarios in total. The oscillation disturbance adds to the system at $t = 0s$. Considering randomness in system load, the frequency of forced oscillation source and damping factor of each generator, 4000 samples are generated. The ratio of training data sets and testing data sets is 1:1. Gaussian White Noise with the signal-to-noise ratio equaling to 13dB is superimposed to the simulated PMU measurements. The testing time series begins at $d = 4s$.

Table 3.3 presents the oscillation source location performance of proposed approach. Another machine learning approach, CELL&Decision tree approach from [63], is employed as comparison. From table 3.3, the overall accuracy of proposal is 97.8%, while the accuracy of several scenarios reaches 100%, satisfying the accurate positioning request of engineering practice. In each scenario, the proposal outperforms the CELL&Decision method.

Table 3. 3 Performance test of oscillation source identification for IEEE 39-bus system.

Generator with disturbance	Accuracy of proposal/%	Accuracy of CELL&Decision/%
G_1	100	95.7
G_2	100	92.8
G_3	100	98.7
G_4	100	99.3
G_5	92	91.3
G_6	100	100
G_7	100	97.3
G_8	92	90.1
G_9	94	93.3
G_{10}	100	95.7
Average	97.8	95.4

We scrutinize the geographic proximity between the identified and actual source. The 8 failed cases for generator 5, are all miss classified to generator 4. As can be seen in the figure 3.10,

the identified and actual source measurement are geographically close. Thus, the proposed method can effectively narrow the searching space even it failed.

C. Influence of oscillation detection delay

Here the influence of time delay in oscillation detection is analyzed. When forced oscillation occurs, software or system operators need some time to detect it. In our work, testing time series begins at $t = d$ second to emulate the time required for oscillation detection. For IEEE 39-bus system, we have conducted simulations with different values of d. Figure 3.11 illustrates the relationship between the location accuracy and the delay d. As shown in figure 3.11, as delay d increases, the location accuracy declines. This is because the proposed approach localizes oscillation sources mainly based on the dynamic characteristics of features in the transient process. When the oscillation tends to be stable, the characteristic of features becomes indistinct. So the sooner the oscillation is detected, the higher is the accuracy.

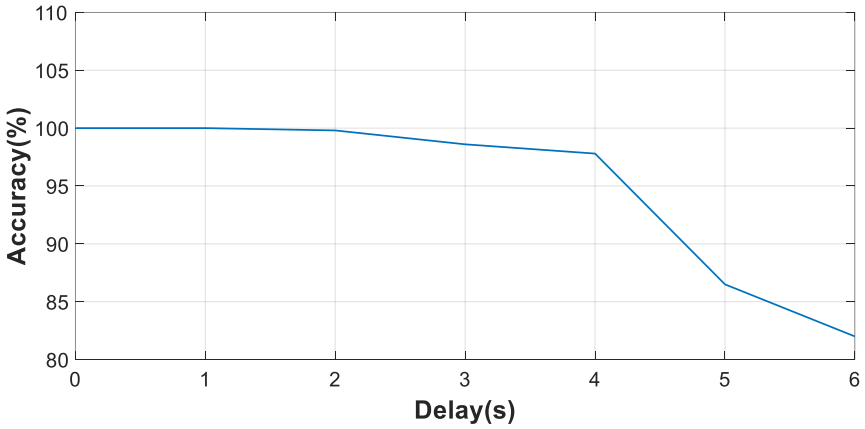

Figure 3. 11 The relationship between location accuracy and the time delay.

3.4 High-Efficiency Forced Oscillation Source Location

Forced oscillation will attenuate rapidly when the disturbance source is removed. The sooner the oscillation source is located and then removed, the less damage to the system will it cause. Timeliness is an important consideration when designing forced oscillation source location

algorithm. On the other hand, k-NN is a classification approach in which efficiency of classification rapidly decreases as the number of instances in training data set increases. Thus, a modified MTS classification based forced oscillation location method with higher efficiency is proposed in this section.

This section is organized as follows: Sub-section 3.4.1 introduces the techniques that can improve the algorithm efficiency. Sub-section 3.4.2 presents results of numerical experiments.

3.4.1 Template Classification

In consideration of algorithm efficiency, a method using the training data set to build MTS templates representing each class, thus reducing the value of I_1, and then classifying the unknown objects based on their Mahalanobis distance to these templates has been proposed.

Instead of computing the average of MTS in each class, instance, which is MTS in this work, with the minimum sum distance of all other instances in the same class to it is chosen as the template. In other word, the template is the instance mostly centrally located in the class. This method is more robust to noise and outliers compared to choosing average of all instances in the class as templates, because it minimizes a sum of pairwise distances instead of a sum of distances. To further improve the robustness and accuracy of the proposed algorithm, a certain number of templates for each class can be selected to form the new training data sets.

For each class, randomly select one instance in the training data set as the initial template. Assuming there are n instances in the class, define the cost as the sum of Mahalanobis distance from data points in the same class to the selected template, expressed as:

$$\mathrm{C}_t = \sum_{j=1}^{J} D_M(\mathbf{X}_i^t, \mathbf{X}_i^j) \tag{3.46}$$

where C_t denotes the cost when instance X_i^t is selected as the template, $\mathbf{X}_i^j$ represents the j th instance in the same class in the training data set.

As shown in figure 3.12, assume the number of template is 1, for each class we choose one MTS, which is most centrally located in that class, as the template.

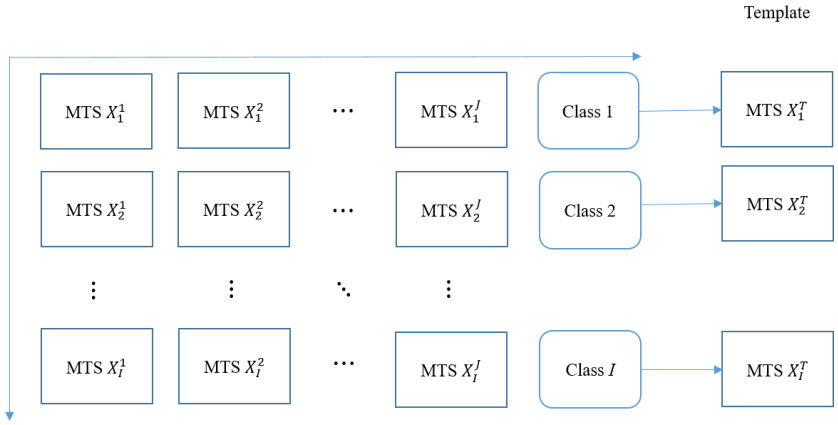

Figure 3. 12 Template generation process.

Swap the template by one of the non-template instance, then recalculate the cost. If the cost increased, undo the swap. The iterative process continues until all instances in the class has been visited. By removing the found template and rerunning the algorithm several times, specific number of templates can be extracted to generate the new training data set. The template generation process can be described as follows:

Table 3. 4 Template generation.

Algorithm 2 Template Generation	
1:	$k = 1, j = 1$
2:	while $k < N\_template$
3:	Randomly choose one instance as initial template
4:	while $j < n$
5:	Calculate the cost using (3.46)
6:	Swap template with non-template instance and
7:	If the cost increases, undo the swap
8:	$j = j + 1$
9:	end
10:	Remove the template
11:	$k = k + 1, j = k$
13:	end

The targeted number of templates is N_template. After applying Algorithm 2 to all classes, a group of templates for each class can be generated to form a new and reduced-size training data set. An unknown object will be classified using Mahalanobis distance to measure the closeness to the new training data sets. With a smaller size of the training data set, the execution time of online classification can be reduced significantly. Both the efficiency and extensibility of the proposed algorithm are improved.

On the other hand, an improved k-NN is used to further improve the algorithm efficiency. Using Mahalanobis distance metric and extended DTW, the distance of out-of-sync MTS can be measured properly. Then k-NN is utilized to assign class membership to an unknown instance by a majority vote of its nearest neighbors. The misclassification rate of the k-NN rule approaches the optimal Bayes error rate asymptotically as k increases [76].

As mentioned before, k-NN is a computational inefficiency classification approach. Typically k is quite small in real application, if the length of time series is H, the number of instances in training set is m_1, the computational complexity of k-NN is about O(m_1H), linear in both the total number of instances and time series length. In consideration of real-time capability of the algorithm, template generation has been applied to reduce the size of training data sets. To further accelerate the execution of the algorithm, space partitioning tree is utilized [77], with which the computational complexity is reduced to O(Hlogm_1) at the price of more memory space.

Figure 3.13 illustrates the procedure of proposed approach. In offline training phase, training data sets are created through time domain simulation. Then with the labeled training date sets Mahalanobis matrix can be learned through algorithm 1. At last, templates, which are mostly centrally located instances in each class, are generated to form the new training data set. When forced oscillation detected, specific PMU measurements are collected to establish testing datasets.

DTW is applied to handle the out-of-sync between testing data and training data sets due to the oscillation detection delay. By comparing the distance, a class label, which is in correspondence to the location of forced oscillation source, is assigned to the testing data.

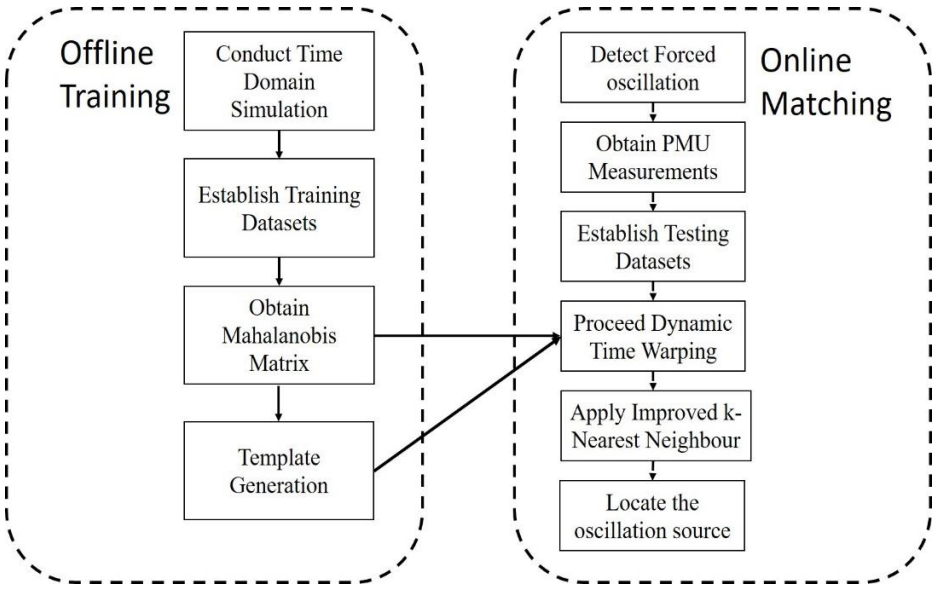

Figure 3. 13 Flowchart of forced oscillation source identification based on multivariate time series classification.

3.4.2 Numerical Experiments

The proposed high-efficiency approach is tested on the modified WECC 179-bus system in the presence of forced oscillation.

The modified WECC 179-bus system is used to illustrate the development of this method. We assume that a PMU is installed at each of the 29 generator bus. The sampling rate of each PMU is 25 data points per second (i.e., $\Delta t = \frac{1}{25}$ s).

A. Data Generation

The simulation setting is similar with the test case library provided by the IEEE PES Task Force on Oscillation Source Location [78]. According to the eigenvalue analysis, one oscillation mode with the frequency at 0.86 Hz exists in this system. As shown in figure 3.8, a scaled 0.86Hz sinusoid disturbance is added to the reference signal of the excitation system attached to the source

generator. In this work, forced oscillation with only one oscillation source is considered. There are 29 generators in WECC 179-bus system, thus 29 possible sources exist.

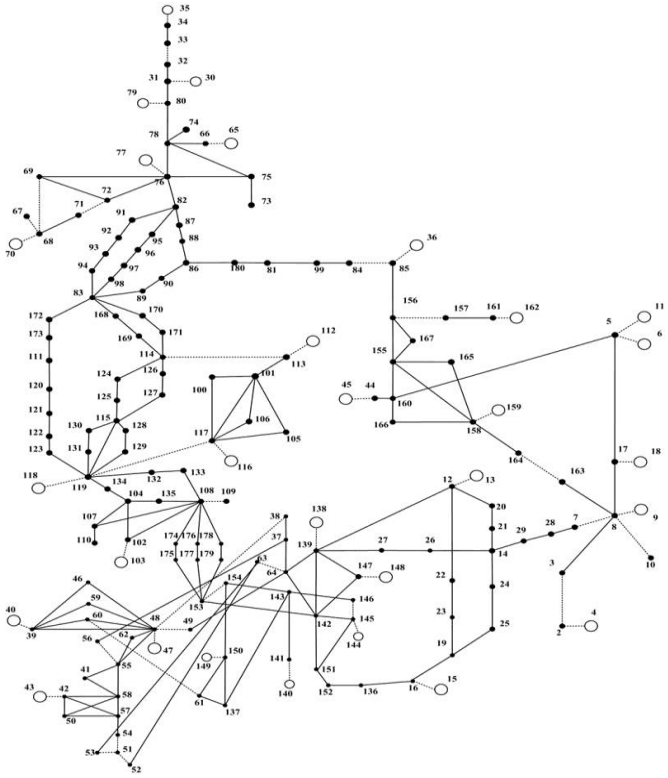

Figure 3. 14 WECC-179 bus system.

Since the data provided by IEEE test case archive is a single snapshot of the state of power system, to emulate practical situation, load fluctuations, which follow the Ornstein-Uhlenbeck process [79], are added to all PQ loads:

$$\dot{u}(t) = -Cu + \sigma\bar{\xi} \tag{3.47}$$

where C is a diagonal matrix of inverse time correlations. $\bar{\xi}$ is a vector of independent standard Gaussian random variables, $\sigma = 0.01$ denotes intensity of noise.

For each scenario, only one generator is injected with the oscillation disturbance. The periodic perturbation begins at time t=0s. The sampling rate of PMU is set as 25Hz. After simulating the system for 24s, PMU measurements, which include terminal voltage (pu), active

power (MW), reactive power (MVAR), absolute angle (deg) and speed (Hz), of each generator are generated. Thus for each instance, a MTS expressed as equation (3.22) with the dimension of rows as h=600 (25×24), the dimension of columns as p=145 (5×29) is generated. To make the simulation more practical, Gaussian White Noise with the signal-to-noise ratio as 13dB is superimposed to the simulated PMU measurements. Considering above-mentioned load fluctuations, 5800 instances (200 instances for each scenario) are generated.

Figure 3.15 shows the simulated PMU measurements of absolute angle of generator 1 (G1) under different conditions. Figure 3.15 (a) illustrates absolute angle measurement when the oscillation disturbance injected at different generators. The plot shows distinct dynamic characteristics for different oscillation source locations, which lays foundation for our locating approach. Another observation is that the oscillation tends to become stable after a certain period, and the characteristics of features for different scenarios become indistinct. This means the measurements in early phase of oscillation are more informative for oscillation source location. Figure 3.15 (b) is the absolute angle measurement when the oscillation disturbance injected at the same generator, but with different system load conditions.

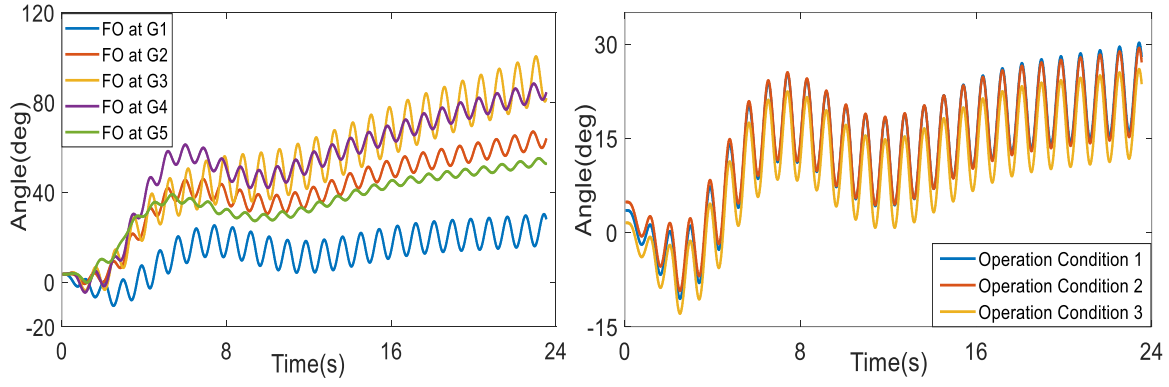

(a) (b)

Figure 3. 15 Simulated PMU measurements. (a) Absolute angle of G1 with disturbance injected at different generators; (b) Absolute angle of G1 with disturbance injected at G1 for different load fluctuations.

We can find the dynamic characteristics keep almost the same, except a small difference in the amplitude of oscillation. To summary, it's possible to classify the MTS made up by PMU measurments, i.e. locating the oscillation source, under different load conditions.

B. Performance Validation

The forced oscillation source location problem has been converted to a multiclass classification problem as the number of classes equals to 29 for WECC 179-bus system. The ratio of training data sets and testing data sets is 1:1. ρ in equation (15) is set as 0, since Mahalanobis matrix learning is learnt offline, thus not a time-critical task, I_1 is set as the size of training data sets (2900), while I_2 as 10. Five features for each generator are recorded, however some of these features may be either redundant or irrelevant. Thus, feature selection, which is the process of selecting a subset of relevant features, is performed. Here, sequential feature selection, which adds features from a candidate subset while evaluating the classification accuracy, is applied. Through the experiments three features are selected: generator active power, absolute angle and speed. For training data sets, the time series begins at t=0s and ends at t=12s. The size of training instance is 300×87. While for testing data sets, a delay d is introduced, which corresponds to the time needed for oscillation detection. Therefore, the oscillations in the test data begins at t=0, and the data fed into the classifier begins at t=d seconds, and the window size is 6s. Thus, the size of testing instance is 150×87.

First, we consider the ideal condition, where there is no oscillation detection delay (assumption for most of existing literatures), i.e. d=0 and all the instances in the training data sets are utilized. Metric learning process is conducted to train Mahalanobis matrix utilizing the whole training data sets. Since d=0, training data sets and testing data sets are synchronized, DTW is applied to map time series with different lengths. Then k-NN classification is utilized to assign

category label to the testing instance, here we consider the number of neighbors k changes from 1 to 10 and compare the precision of classification. Figure 3.16 shows the precision of classification for different value of k. The highest accuracy is 97.71% when k=1, while the lowest accuracy is 96.8% when k=10. There is no big diffidence in precision of classification with respect to different values of k, as k varies from 1 to 10, accuracy oscillates in a range of 0.0091%. For simplicity, in the following analysis, k is set to 1 to conduct online matching. For all 29 scenarios, the highest accuracy is 100%, while the lowest accuracy is 93.3%, satisfying the accurate positioning request of engineering practice. The online matching time is 5.6s as k=1 for each testing instance on a PC (3.7Ghz Intel Core i7 processer with 32GB RAM).

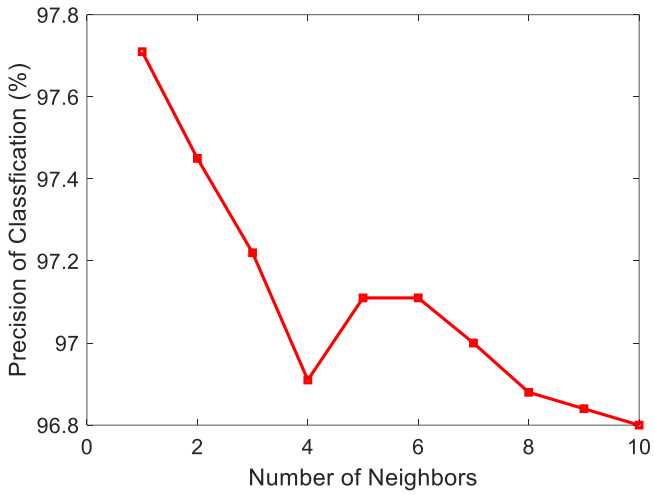

Figure 3. 16 Precision of classification for ideal case.

C. Performance of Template Classification

Forced oscillation will attenuate rapidly when the disturbance source is removed. The sooner the oscillation source is located and then removed, the less damage to the system will it cause. Timeliness is an important consideration when designing forced oscillation source location algorithm. On the other hand, k-NN is a classification approach in which efficiency of classification rapidly decreases as the number of instances in training data set increases. Thus, the

template generation and classification method has been proposed to increase the algorithm efficiency. Two criteria will be utilized to evaluate the performance of the template classification method-the classification accuracy and the online matching time. The ideal case-all the instances in the training data sets are utilized to conduct online matching is used as a benchmark (i.e. 100 instances for each class).

Algorithm 2 has been utilized to generate templates for each scenario, and k-NN with k=1 is applied. It means a testing instance O_i(whose class label is unknown) shall be assigned to a class represented by template $X_{i_T}^{j_T}$ if distance of O_i with $X_{i_T}^{j_T}$ is minimum compared the ones between the test instance and all other templates. The simulation results are listed in table 3.5:

Table 3. 5 The performance of different number of templates.

	Precision of Classification(%)	Time for Online Matching(s)
Benchmark	97.7	5.603
1 template	95.94	0.058
2 templates	95.94	0.113
3 templates	95.52	0.175
4 templates	96.05	0.217
5 templates	96.21	0.261
6 templates	95.75	0.331

Various number of templates are considered and tested. As can be seen from the table, the precision of classification keeps high even with much lesser instances in training data sets. In the meantime, the time needed for online matching declines dramatically. For example, compare the case of one template for each scenario and the benchmark, the online matching time is 5.545 seconds less, reduced by 98.96%. While the precision of classification changes from 97.7% to 95.94%, decreased by 1.76%. Also, as expected the smaller the number of templates for each scenario, the less of time needed for online matching. Using the information listed in table 3.5, we plot the figure 3. 17. The left y axis shows the precision of classification, and the right y axis

illustrates the execution time. As can be seen from the figure, execution time is linearly increased as with respect to the number of templates.

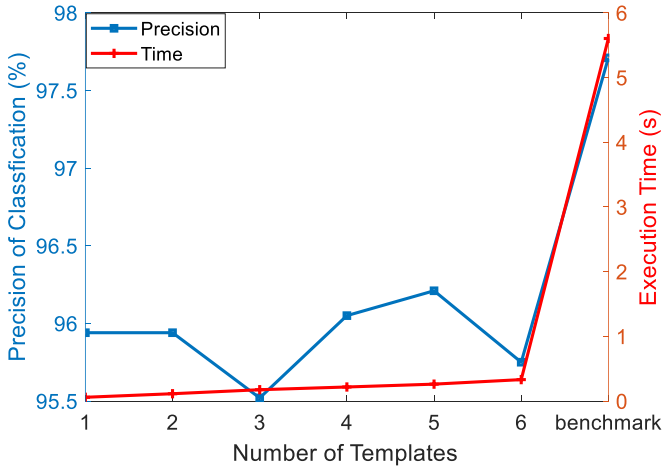

Figure 3. 17 Precision and execution time for different number of templates.

By implementing template classification, the algorithm can locate the oscillation source in an online fashion with a relatively high accuracy, satisfying the timeliness requirement. As analyzed in section III part B, the computational complexity is O(Hlogm_1) with H is the length of time series, m_1 is the number of instances in training set. For a larger system with 500 generators, the online matching time with number of templates selected as 1 could be estimated about 0.1102 seconds. The algorithm is readily applicable for larger system. Typically, more instances in training data sets would lead to a higher classification accuracy. Thus, there is a tradeoff between classification precision and execution time when selecting the number of templates.

D. Influence of oscillation detection delay

As shown in figure 3.15(a), the measurements in early phase of the oscillation have more distinct characteristics for different locations of sources. However, accurately detecting the beginning time of oscillations after disturbance is not practical. In this part the influence of time delay needed by oscillation detection is analyzed. Testing time series begins at t=d second to

emulate errors in locating the beginning point of oscillations. The number of templates for each scenario is set to 1. Figure 3.18 illustrates the relationship between the location accuracy and the delay d. As delay d increases, the location accuracy declines. When d=5s, the location accuracy becomes 74.07%, decreased by 23.32% compared with the ideal case. This is because the proposed approach localizes oscillation sources mainly based on the dynamic characteristics of features in the transient process. When the oscillation tends to be stable, the characteristic of features becomes indistinct. So, the sooner the oscillation is detected, the higher is the location accuracy.

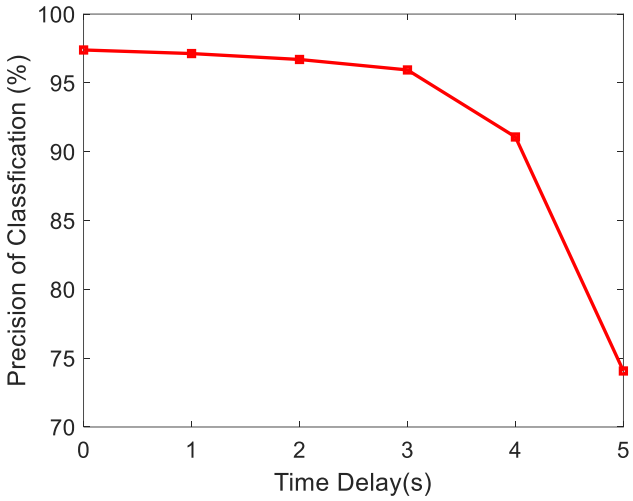

Figure 3. 18 Precision of classification over different *d*.

E. Performance for harmonics

One of the major differences between the poorly damped oscillation and forced oscillation is the harmonic nature of forced oscillation [80]. In this subsection, harmonic disturbance injected to the excitation system of the source generator are considered. The fundamental frequency is still at 0.83Hz. As shown in figure 3.19, the harmonics is added to the excitation system of the source generator. The source generator is selected randomly as generator at bus 4, generator at bus 79 and generator at bus 162, respectively. Following Ornstein-Uhlenbeck process, 10 instances with

different load conditions for each scenario are generated. There can be numerous combinations of harmonics with the same fundamental component. Thus, to test the performance of proposed approach for harmonics, no harmonic cases are put into the training data sets. Harmonic cases only exist in testing data sets.

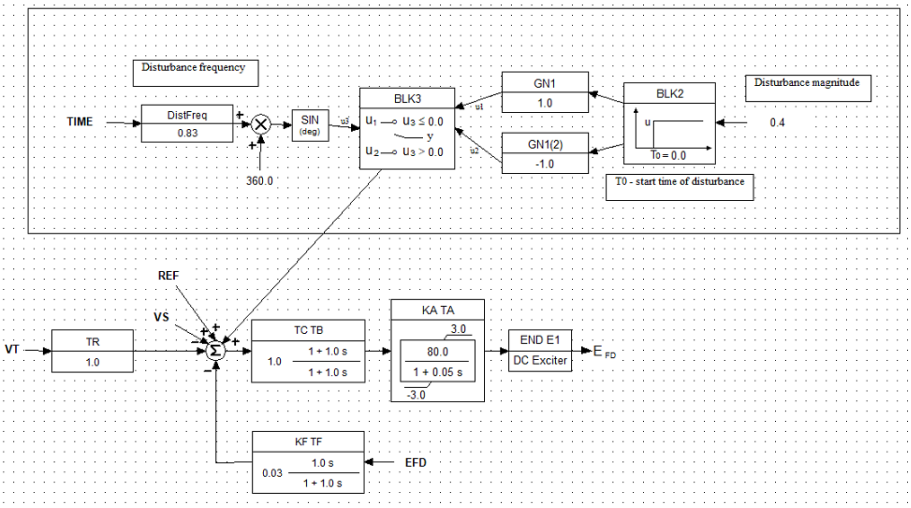

Figure 3. 19 Process to add harmonic oscillation source.

Set the number of templates for each scenario as 1 and d=2s. The overall accuracy for the harmonic cases is 86.67% (70% for generator at bus 4, 90% for generator at bus 79 and 100% for generator at bus 162). The precision of classification does drop compared with the same simulation setting of non-harmonic cases in part D. However, the proposed algorithm still gives a good indication of the oscillation source when harmonics exist. This indicates that the proposal is robust to situations when harmonics exist.

3.4.3 Conclusions

In this section, a multivariate time series classification method to locate the forced oscillation sources in power systems has been proposed. Mahalanobis distance of MTS constructed by rotor angle and active power of each generator is obtained through metric learning. Dynamic time warping is applied to find the optimized warping path for time series with different phases or

lengths. After that, the real-time measurements can be utilized to determine the forced oscillation source by comparing the Mahalanobis distance between the testing data and the training data. Because MTS integrates all information during the transient process, it can represent the forced oscillation characteristic caused by different oscillation disturbance very well. Experimental results show the proposed approach has high location accuracy. Considering practical applications, the relationship between oscillation detection delay and detection accuracy is investigated.

The proposed approach works well for forced oscillation. In subsequent work, we hope to leverage the MTS and machine learning technique to distinguish forced oscillation and poorly damped oscillation. Then the correct remedial reactions to mitigate the negative impacts of oscillations can be effectively implemented.

CHAPTER 4 SUMMARY

Motivated by the maturing of ESS technology and increasing amount of ESS installed in power system, the research work has been conducted on the application ESS can be used for in two sub-areas: regulation service which is aiming to maintain a continuous balance between generation and load, mitigation of forced oscillation which is an essential guarantee for the secure and stable operation of power system. The work in each sub-area is abridged as follows:

A. Providing regulation service

First, a cost benefit study of using ESS to provide regulation services is performed. The impact of lifetime depreciation characteristics and regulation signal design on ESS service lifetime depreciation, service quality and service costs are quantified. Two ESS operation mechanisms are considered: 1-directional and 2-directional services. When providing 1-directional service, the ESS only responds to regulation-up or regulation-down service during the committed period. When providing 2-directional service, the ESS can respond to both regulation-up and regulation-down signals. Regulation and price data published by New York Independent System Operator and PJM are used to conduct the study. The simulation results show that it's feasible and beneficial to provide regulation service using ESS. From the perspective of ISO/RTO, the quality of the service will be improved while the total regulation procurement can drop when ESS take part in the regulation market, due to the supreme ramp rate of ESS. From the perspective of ESS owner, participating in regulation market is profitable, even considering the life time depreciation.

Then, an energy storage friendly regulation signal design method based on EMD has been proposed. BESS have very fast response rate and excellent ramping capability, making them ideal resources for providing fast regulation services. However, the limitation in energy storage capacity prevents the BESS from following non-energy neutral signals for prolonged durations. The

proposed EMD-based approach decomposes the raw regulation signal into an energy-neutral, fast-changing component and a slow-changing component that reflects the overall trend. Simulation results and the cost benefit study all demonstrate that both generators and BESSs have achieved better performance in terms of revenue, response rate, and lifetime when responding to the EMD-based regulation signals compared with the filter-based RegA and RegD signals.

B. Mitigation of forced oscillation

Forced oscillation could happen even when the grid is with good damping factor, which may damage electrical equipment and even lead to a crash of the whole system. The most effective way to deal with forced oscillation is to locate and remove the oscillation source. However, both the detection of oscillation and location of oscillation source need time. A novel approach which can damp the oscillation is introduced first. Assume STATCOM incorporated with ESS is installed in the system, a control strategy utilizing resonant controllers whose outputs are the power references of E-STATCOM is adopted. However this damping method also needs the identification of the location of the forced oscillation source.

With the intuition that different locations of oscillation source would lead to distinct characteristics in PMU measurements through the whole system, a forced oscillation source location method based on MTS classification is proposed in this paper. The location problem is converted to a MTS classification problem while the class membership corresponds to the location of oscillation source. PMU measurements of each generation are recorded, through sequential feature selection the most informative measurements are selected and utilized to construct MTS. Mahalanobis metrics are trained to represent the distance between MTS accordingly. With the obtained distance metric, templates representing each class are constructed to improve the algorithm efficiency. DTW is applied thus MTS of different lengths and phases can be

appropriately compared which relaxes the assumption of accurate detection of the beginning of oscillations. Simulation results on four-machine two-area and IEEE 39-bus system have shown the effectiveness of the proposed method. Then considering the efficiency of the approach, templates generation and improved kNN are used to reduce the execution time. Numerical experiments on WECC 179-bus system demonstrate the improved approach can maintain a high location accuracy while reducing the calculation time dramatically.

REFERENCES

[1] M. H. Rashid, Electric renewable energy systems. Elsevier, 2016.

[2] "DOE global energy storage database," [Online]. Available: https://www.energystorageexchange.org/

[3] NC State Energy Storage Team, "Energy storage options for North Carolina," [Online]. Available: https://energy.ncsu.edu/storage/wp-content/uploads/sites/2/2018/12/NC-Storage-Study-FINAL.pdf.

[4] T. Qiu, B. Xu, Y. Wang, Y. Dvorkin, and D. S. Kirschen, "Stochastic multistage coplanning of transmission expansion and energy storage," IEEE Trans. Power Syst., vol. 32, no. 1, pp. 643–651, Jan. 2017.

[5] B. Nykvist and M. Nilsson, "Rapidly falling costs of battery packs for electric vehicles," Nat. Clim. Change, vol. 5, no. 4, pp. 329–332, Apr. 2015.

[6] "Battery storage for renewables: market status and technology outlook," [Online]. Available: /publications/2015/Jan/Battery-Storage-for-Renewables-Market-Status-and-Technology-Outlook.

[7] "Energy storage exchange." [Online]. Available: https://www.energystorageexchange.org/.

[8] "U.S. battery storage market trends," [Online]. Available: https://www.eia.gov/analysis/studies/electricity/batterystorage/pdf/battery_storage.pdf

[9] Leitermann O (2012). Energy storage for frequency regulation on the electric grid. Ph.D. dissertation, Dept. Elect. Eng. Commun. Sci., Massachusetts Inst. Technol., Cambridge, MA, USA, Ch. 1 and 2.

[10] "PJM - ancillary services." [Online]. Available: https://www.pjm.com/markets-and-operations/ancillary-services.aspx.

[11] “Energy market & operational data - NYISO.” [Online]. Available: https://www.nyiso.com/energy-market-operational-data.

[12] North American Electric Reliability Corporation Std. BAL-001-2(2008). Real power balancing control performance. [Online]. Available: https://www.nerc.com/pa/Stand/Reliability%20Standards/BAL-001-2.pdf.

[13] P. Kundur, Power system stability and control. The EPRI power system engineering series. McGraw-Hill, 1994.

[14] B. WANG and K. SUN, “Location methods of oscillation sources in power systems: a survey,” J. Mod. Power Syst. Clean Energy, vol. 5, no. 2, pp. 151–159, Mar. 2017.

[15] D. Song, X. Yang, Q. Ding, et al., “A survey on low-frequency oscillation in large-scale inter-connected power grid and its control measures,” Power System Technology, vol. 35, no. 10, pp. 22-27, 2011.

[16] S. A. N. Sarmadi and V. Venkatasubramanian, “Inter-Area resonance in power systems from forced oscillations,” IEEE Trans. Power Syst., vol. 31, no. 1, pp. 378–386, Jan. 2016.

[17] M. Beza and M. Bongiorno, “An adaptive power oscillation damping controller by STATCOM with energy storage,” IEEE Trans. Power Syst., vol. 30, no. 1, pp. 484–493, Jan. 2015.

[18] P. Jiang, S. Feng, and X. Wu, “Robust design method for power oscillation damping controller of STATCOM based on residue and TLS-ESPRIT,” Int. Trans. Electr. Energy Syst., vol. 24, no. 10, pp. 1385–1400, 2014.

[19] S. Feng, X. Wu, P. Jiang, L. Xie, and J. Lei, “Mitigation of power system forced oscillations: an E-STATCOM approach,” IEEE Access, vol. 6, pp. 31599–31608, 2018.

[20] North American Electric Reliability Corporation, Balancing and frequency control [Online]. Available: https://www.nerc.com/docs/oc/rs/NERC%20Balancing%20and%20Frequency%20Control%20040520111.pdf

[21] G. Zhang, J. D. McCalley, "Estimation of regulation reserve requirement based on control performance standard," IEEE Trans. Power Syst., vol. 33, no. 2, pp. 1173–1183, Mar. 2018.

[22] ISO-NE, "Final report: New England wind integration study", Dec. 2010. [Online]. Available: https://www.iso-ne.com/static assets/documents/committees/comm_wkgrps/prtcpnts_comm/pac/reports/2010/newis_report.pdf.

[23] FERC, "Frequency regulation compensation in the organized wholesale power markets (order no. 755)". [Online]. Available: https://www.ferc.gov/whats-new/comm-meet/2011/102011/E-28.pdf

[24] "State of charge: Massachusetts energy storage initiative." [Online]. Available: https://www.mass.gov/files/2017-07/state-of-charge-report.pdf

[25] B. Xu, Y. Dvorkin, D. S. Kirschen, C. A. Silva-Monroy, and J. Watson, "A comparison of policies on the participation of storage in U.S. frequency regulation markets," in 2016 IEEE Power and Energy Society General Meeting (PESGM), 2016, pp. 1–5.

[26] "PJM Manual 12: Balancing Operations," PJM, 2018. [Online]. Available: https://www.pjm.com/-/media/documents/manuals/m12.ashx

[27] Kleinman Center for Energy Policy, "Energy storage in PJM." [Online]. Available: https://kleinmanenergy.upenn.edu/sites/default/files/Energy%20Storage%20in%20PJM.pdf

[28] PJM State & Member Training Department (2016). “Regulation,” [Online]. Available: https://www.pjm.com/-/media/training/nerc-certifications/markets-exam-materials/mkt-optimization-wkshp/regulation-market.ashx?la=en

[29] D. Stroe, V. Knap, M. Swierczynski, A. Stroe, and R. Teodorescu, “Operation of a grid-connected lithium-ion battery energy storage system for primary frequency regulation: A Battery Lifetime Perspective,” IEEE Trans. Ind. Appl., vol. 53, no. 1, pp. 430–438, Jan. 2017.

[30] G. Ning and B. N. Popov, “Cycle life modeling of lithium-ion batteries,” J. Electrochem. Soc., vol. 151, no. 10, pp. A1584–A1591, Oct. 2004.

[31] V. Ramadesigan, P. W. C. Northrop, S. De, S. Santhanagopalan, R. D. Braatz, and V. R. Subramanian, “Modeling and simulation of lithium-ion batteries from a systems engineering perspective,” J. Electrochem. Soc., vol. 159, no. 3, pp. R31–R45, Jan. 2012.

[32] Q. Zhai, K. Meng, Z. Y. Dong, and J. Ma, “Modeling and analysis of lithium battery operations in spot and frequency regulation service markets in Australia electricity market,” IEEE Trans. Ind. Inform., vol. 13, no. 5, pp. 2576–2586, Oct. 2017.

[33] B. Xu, Y. Shi, D. S. Kirschen, and B. Zhang, “Optimal battery participation in frequency regulation markets,” IEEE Trans. Power Syst., vol. 33, no. 6, pp. 6715–6725, June 2018.

[34] P. Ruetschi, “Aging mechanisms and service life of lead–acid batteries,” J. Power Sources, vol. 127, no. 1, pp. 33–44, Mar. 2004.

[35] X. Ke, N. Lu, and C. Jin, “Control and size energy storage systems for managing energy imbalance of variable generation resources,” IEEE Trans. Sustain. Energy, vol. 6, no. 1, pp. 70–78, Jan. 2015.

[36] D. Fooladivanda, C. Rosenberg, and S. Garg, “Energy storage and regulation: an analysis,” IEEE Trans. Smart Grid, vol. 7, no. 4, pp. 1813–1823, Jul. 2016.

[37] Y. Meng, M. Liang, and N. Lu, “A cost benefit study of using energy storage ti provide regulation services,” IEEE ISGT, Washington D.C., Feb., 2019 .

[38] “FERC orders on PJM’s frequency regulation market give energy storage providers another recent win,” Akin Gump Strauss Hauer & Feld LLP. [Online]. Available: https://www.akingump.com/en/experience/industries/energy/speaking-energy/ferc-orders-on-pjm-s-frequency-regulation-market-give-energy.html.

[39] “Description of the energy neutral AGC dispatch algorithm,” [Online]. Available: https://www.iso-ne.com/static-assets/documents/2015/03/energy_neutral_dispatch_algorithms.pdf

[40] Implementation and rationale for PJM’s conditional neutrality regulation signals, PJM, Jan.2017. [Online]. Available: https://www.pjm.com/~/media/committees-groups/task-forces/rmistf/postings/regulation-market-whitepaper.ashx.

[41] Huang Norden E. et al., “The empirical mode decomposition and the Hilbert spectrum for nonlinear and non-stationary time series analysis,” Proc. R. Soc. Lond. Ser. Math. Phys. Eng. Sci., vol. 454, no. 1971, pp. 903–995, Mar. 1998.

[42] C. Jin, N. Lu, S. Lu, Y. V. Makarov, and R. A. Dougal, “A coordinating algorithm for dispatching regulation services between slow and fast power regulating resources,” IEEE Trans. Smart Grid, vol. 5, no. 2, pp. 1043–1050, Mar. 2014.

[43] S. Tolwinski, “The Hilbert transform and empirical mode decomposition as tools for data analytics” [Online]. Available: http://math.arizona.edu/~flaschka/Topmatter/527files/termpapers/suz.pdf.

[44] Y. Meng, M. Liang, J. F. DeCarolis and N. Lu, “Design of energy storage friendly regulation signals using empirical mode decomposition,” PES General Meeting, Atlanta, GA, Aug. 2019.

[45] D. Newbery, “Shifting demand and supply over time and space to manage intermittent generation: The economics of electrical storage,” Energy Policy, vol. 113, pp. 711–720, Feb. 2018.

[46] D. N. Kosterev, C. W. Taylor, and W. A. Mittelstadt, “Model validation for the August 10, 1996 WSCC system outage,” IEEE Trans. Power System, vol.14, no.3, pp. 967-979, Aug. 1999.

[47] X. Wang, K. Turitsyn, “Data-driven diagnostics of mechanism and source of sustained oscillations,” IEEE Trans. Power System, vol. 31, no. 5, pp. 4036-4046, Sep. 2016.

[48] J. Ma, P. Zhang, H. J. Fu, et al., “Application of phasor measurement unit on locating disturbance source for low-frequency oscillation,” IEEE Trans. Smart Grid, vol. 1, no. 3, pp. 340-346, Oct. 2010.

[49] N. Zhou and J. Dagle, “Initial results in using a self-coherence method for detecting sustained oscillations,” IEEE Trans. on Power Systems, vol. 30, no. 1, pp. 522-530, 2015.

[50] “Forced oscillations,” [Online]. Available: https://phys.libretexts.org/Bookshelves/University_Physics/Book%3A_University_Physics_(OpenStax)/Map%3A_University_Physics_I_-_Mechanics%2C_Sound%2C_Oscillations%2C_and_Waves_(OpenStax)/15%3A_Oscillations/15.6%3A_Forced_Oscillations

[51] M. A. Magdy and F. Coowar, “Frequency domain analysis of power system forced oscillations,” in IEE Proceedings C-Generation, Transmission and Distribution, vol. 137, no. 4 IET 1990, pp. 261-268.

[52] M. Ghorbaniparvar, “Survey on forced oscillation in power system,” J. Mod. Power Syst. Clean Energy, vol. 5, no. 5, pp. 671-682, Sep. 2017.

[53] D. S. L. Dolan and P. W. Lehn, “Simulation model of wind turbine 3p torque oscillations due to wind shear and tower shadow,” IEEE Trans. Energy Convers., vol. 21, no. 3, pp. 717-724, Sep. 2006.

[54] C. Su, W. Hu, Z. Chen, and Y. Hu, “Mitigation of power system oscillation caused by wind power fluctuation,” IET Renew. Power Gener., vol. 7, no. 6, pp. 639-651, Nov. 2013.

[55] Y. Yu, Y. Min, L. Chen, and Y. Zhang, “Analysis of forced power oscillation caused by continuous cyclical load disturbances,” Automation of Electric Power Systems, vol. 34, pp. 7-11, Mar. 2010.

[56] S. Achanta, M. Danielson, P. Evans, et al., “Time synchronization in the electric power system,” North American synchrophasor Initiative, Tech Report NAPSI-2017-TR-001, March 2017.

[57] P. N. Markham and Y. Liu, “Electromechanical wave propagation in large electric power systems,” IEEE Trans. Circuits Syst. I, Fundam. Theory, vol.45, no.6, pp.614-622, Jun. 1998.

[58] L. Chen, Y. Min, and W. Hu, “An energy-based method for location of power system oscillation source,” IEEE Trans. Power Syst., vol.28, no.2, pp.828–836, May 2013.

[59] S. Maslennikov, B. Wang, and E. Litvinov, “Dissipating energy flow method for locating the source of sustained oscillations,” Int. J. Elect. Power Energy Syst., vol. 88, pp. 55-62, Jun. 2017.

[60] S. Chevalier, P. Vorobev, K. Turitsyn, “Using effective generator impedance for forced oscillation source location,” IEEE Trans. Power Syst., vol. 33, no. 6, May 2018.

[61] L. Dosiek, N. Zhou, J. W. Pierre, Z. Huang, and D. J. Trudnowski, “Mode shape estimation algorithms under ambient conditions: A comparative review,” IEEE Trans. Power Syst., vol. 28, no. 2, pp. 779–787, May 2013.

[62] X. Yang, D. Liu, Q. Liao, et al., “Application of dynamic approximate entropy in real-time detection of forced power oscillation,” Power System Technology, vol.36, no.11, pp.129-133, 2012.

[63] C. Jiang, J. Liu, Y. Liu, et al., “Online forced oscillation detection and identification based on wide area measurement system and CELL theory,” Electric Power Automation Equipment, vol.35, no.2, pp.125-132, Feb. 2015.

[64] https://www.dsatools.com/

[65] Y. Meng, Z. Yu, D. Shi, et al., “Forced oscillation source location via multivariate time series classification,” IEEE/PES Transmission and Distribution Conference and Exposition, Denver, CO, April 16-19, 2018.

[66] S. S. Tsai, et al., "Study of global frequency dynamic behavior of large power systems," in Power Systems Conference and Exposition, 2004. IEEE PES, 2004, pp. 328-335 vol.1.

[67] J. Mei, M. Liu, Y. Wang, and H. Gao, “Learning a Mahalanobis distance-based dynamic time warping measure for multivariate time series classification,” IEEE Trans. Cybern., vol.46, no.6, pp.1363-1374, May 2015.

[68] J. Bi, D. Wu, L. Lu, M. Liu, Y. Tao, and M. Wolf, “Adaboost on low-rank psd matrices for metric learning,” IEEE Conference on Computer Vision and Pattern Recognition, IEEE, 2011, pp. 2617-2624.

[69] J. V. Davis, B. Kulis, P. Jain, S. Sra, and I. S. Dhillon, “Information-theoretic metric learning,” in Proceedings of the 24th international conference on Machine Learning. ACM, 2007, pp. 209-216.

[70] M. Sugiyama, “Dimensionality reduction of multimodal labeled data by local fisher discriminant analysis,” The Journal of Machine Learning Research, vol. 8, pp. 1027-1061, 2007.

[71] J. Mei, M. Liu, H. R. Karimi, and H. Gao, “Logdet divergence based metric learning with triplet constraints and its applications,” IEEE Trans. on Image Process., vol. 23, no. 11, pp. 4920 – 4931,2014.

[72] B. Kulis, M. Sustik, and I. Dhillon, “Learning low-rank kernel matrices,” in Proceedings of the 23rd international conference on Machine learning. ACM, 2006, pp. 505–512.

[73] J. Mei, M. Liu, Y. Wang, and H. Gao, “Learning a Mahalanobis distance-based dynamic time warping measure for multivariate time series classification,” IEEE Trans. Cybern., vol. 46, no. 6, pp. 1363–1374, Jun. 2016.

[74] M. Muller, “Dynamic time warping,” Information Retrieval for Music and Motion, pp.69-84, 2007.

[75] M. A. Pai. Energy function analysis for power system stability. The Kluwer international series in engineering and computer science. Power electronics and power systems. Boston: Kluwer Academic Publishers, 1989.

[76] K. Fukunaga and L. D. Hostetler, “k-nearest-neighbor Bayes-risk estimation,” IEEE Trans. Inform. Theory, no. 21, pp. 285-293, 1975.

[77] M. Otair, “Approximate k-nearest neighbor based spatial clustering using K-D tree,” International Journal of Database Management Systems, vol. 5, no.1, pp. 97-108, 2013

[78] S. Maslennikov, B. Wang, Q. Zhang, F. Ma, X. Luo, K. Sun, E. Litvinov, "A Test Cases Library for Methods Locating the Sources of Sustained Oscillations," IEEE PES General Meeting, Boston, MA, July 17-21, 2016.

[79] G. Ghanavati, P. D. H. Hines, and T. I. Lakoba, "Identifying useful statistical indicators of proximity to instability in stochastic power systems," IEEE Trans. Power System, vol. 31, pp. 1360-1368, March 2016.

[80] R. Xie and D. J. Trudnowski, "Distinguishing Between Natural and Forced Oscillations Using a Cross-Spectrum Index," IEEE PES General Meeting, Chicago, IL, July 16-20, 2017.